Journal Pre-proof

Co-pyrolysis of biomass with phosphate additives: linking phosphorus transformations to nutrient release for tailor-made biochar-based fertilizers

Jesper T.N. Knijnenburg, Kaewta Jetsrisuparb

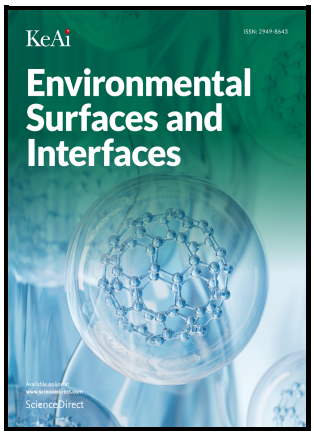

PII: S2949-8643(26)00011-1

DOI: https://doi.org/10.1016/j.esi.2026.03.001

Reference: ESI55

To appear in: *Environmental Surfaces and Interfaces*

Received date: 20 October 2025
Revised date: 6 March 2026
Accepted date: 16 March 2026

Please cite this article as: Jesper T.N. Knijnenburg and Kaewta Jetsrisuparb, Co-pyrolysis of biomass with phosphate additives: linking phosphorus transformations to nutrient release for tailor-made biochar-based fertilizers, *Environmental Surfaces and Interfaces,* (2026) doi:https://doi.org/10.1016/j.esi.2026.03.001

Co-pyrolysis of biomass with phosphate additives: linking phosphorus transformations to nutrient release for tailor-made biochar-based fertilizers

Jesper T.N. Knijnenburg[1] and Kaewta Jetsrisuparb[2]*

[1] International College, Khon Kaen University, Khon Kaen 40002, Thailand

[2] Department of Chemical Engineering, Khon Kaen University, Khon Kaen 40002, Thailand

* corresponding author: Jesper T.N. Knijnenburg

Email: jespth@kku.ac.th

Phone: +66956632001

Abstract

The co-pyrolysis of biomass with phosphates is an emerging strategy for producing advanced biochar-based fertilizers. The properties of these fertilizers, particularly the speciation and release of phosphorus (P), are highly complex and dependent on synthesis parameters. This article provides a comprehensive review on the co-pyrolysis of biomass with well-defined phosphates, including phosphoric acid (H_3PO_4) and salts of ammonium (e.g., $NH_4H_2PO_4$, $(NH_4)_2HPO_4$), sodium (e.g., NaH_2PO_4, Na_2HPO_4, Na_3PO_4), potassium (e.g., KH_2PO_4, K_2HPO_4, K_3PO_4), magnesium (e.g., from H_3PO_4 with MgO), and calcium (e.g., $Ca(H_2PO_4)_2$). Supported by the thermal transformation pathways of these pure phosphates, we identify the key factors governing P transformations during co-pyrolysis: higher pyrolysis temperatures and higher degrees of protonation favor the condensation of orthophosphates into pyro- and polyphosphates. Furthermore, P release kinetics are primarily dictated by cation valency and biomass composition; monovalent cations (e.g., K^+) typically generate highly soluble P forms, whereas divalent cations like Ca^{2+} (either from the additive or present in the biomass feedstock) promote the

formation of poorly soluble P species. The review also discusses specific limitations of the current literature and outlines future research directions. The synthesis of this information provides design principles for engineering biochar-based P fertilizers with targeted release profiles to improve sustainable use of P in agriculture.

KEYWORDS: Pyrolysis, phosphorus, sustainability, carbonization, agriculture, circular economy

1. Introduction

Water-soluble phosphorus (P) fertilizers are heavily applied in agriculture to support the crop demands of the growing world population. However, only a small portion of the applied P is taken up by crops, while the rest of the P is lost to surface water runoff (causing eutrophication) or locked in the soil in plant-unavailable forms [1, 2]. Furthermore, these P fertilizers are primarily prepared from non-renewable phosphate rock deposits that are mainly concentrated in Morocco, Western Sahara, and Norway [3, 4] and could be depleted within 30 to 300 years [5]. To overcome these problems, biochar has emerged as a promising sustainable solution. Biochar is a stable carbon-rich material that is produced by pyrolysis, i.e., the thermal conversion of biomass in an oxygen-limited environment. Biochars can function as slow-release fertilizers with enhanced nutrient use efficiency, resulting in higher crop productivity by 10% over fertilized control [6] and by 15% when combined with inorganic fertilizers [7]. On average, biochars increase P availability to plants by a factor of 4.6 [8].

However, many biochars have low fertilizer value due to the inherent low P concentration of many (lignocellulosic) biomasses. To address this, biochars are often modified with plant nutrients. While post-pyrolysis modification typically results in a fast-release P biochar fertilizer, pre-pyrolysis modification (or co-pyrolysis with a P source) creates a slow-release P fertilizer whose release rate can be tailored by controlling the pyrolysis conditions. In addition to increasing P content, co-pyrolysis with P sources enhances carbon

stabilization [9], the stability of endogenous heavy metals [10], and exogenous heavy metal adsorption/stabilization in water [11] or soil [12]. This approach thus transforms organic waste into a stable, carbon-rich biochar while simultaneously incorporating P into the biochar matrix, which reduces P solubility and leaching and increases overall fertilizer use efficiency.

The speciation and availability of P in biochars are strongly dependent on feedstock composition, pyrolysis conditions, and the nature of the additives. Existing reviews have covered P transformations in various biomasses during (hydro)thermal treatment [13, 14], including pyrolysis of specific wastes such as manure [15] or sewage sludge [16]. To the best of our knowledge, the co-pyrolysis of biomass with exogenous phosphate sources has not been systematically reviewed. This review aims to fill that gap by focusing specifically on phosphate-biomass interactions during pyrolysis. To provide a clear understanding of the fundamental interactions and mechanisms, the scope of this article is defined as follows: (1) this review focuses on pure phosphates because of their well-defined chemical composition, excluding P-rich resources with variable compositions like phosphate rock [17], phosphate tailings [18], wet process phosphoric acid [19], bone meal [20], and manure [21]; (2) this review focuses on P transformations and retention within the biochar, excluding studies that use post-treatment washing or lack biochar characterization ; (3) the scope is limited to co-pyrolysis, excluding studies on post-pyrolysis modification of biochars; and (4) hydrothermal carbonization is excluded because a large fraction of P migrates into the liquid phase [14].

The objectives of this review are: (1) to determine the reaction mechanisms governing P transformations during co-pyrolysis of biomass with specific, well-defined phosphate compounds, specifically analyzing the interaction between phosphate salt additive, feedstock properties, and pyrolysis conditions; (2) to establish structure-function relationships linking the structure of the resulting P species to extractability, release kinetics, and plant uptake; and (3) to critically assess limitations in the literature and identify barriers to the large-scale synthesis and applications of such biochar-based P fertilizers. To address these objectives, Section 2 discusses the general properties and thermal transformations of the pure phosphates. Section 3 then examines the P transformations in co-pyrolysis biochars, while Section 4 evaluates their solubility, kinetic release, and plant

availability. A comparative analysis of transformation mechanisms is presented in Section 5, and Section 6 finally outlines the challenges and future research directions.

2. Properties and transformations of pure phosphates

To understand the P transformations during co-pyrolysis, the inherent properties of the phosphates (namely their chemistry, solubility behavior, and thermal transformations) are briefly reviewed first. This information serves as a fundamental background for interpreting the complex phosphate-biomass interactions discussed in later sections.

2.1. General phosphate chemistry

Inorganic P is most commonly found in the form of phosphates, which exist in several structural forms. The simplest form is orthophosphate (PO_4^{3-}), in which the pentavalent P is bonded to four oxygen atoms (three single bonds, one double bond) in a tetrahedral coordination [22]. Orthophosphoric acid (H_3PO_4) is a water-miscible weak acid [23] with three pKa values (2.16, 7.21, and 12.32) [24] and typically exists as $H_2PO_4^-$ or HPO_4^{2-} ions in aqueous solutions.

Orthophosphate ions form salts with various cations. The solubility of these salts generally negatively correlates with cation charge: phosphates of monovalent cations like Na^+, K^+, and NH_4^+ are highly water-soluble, while those of divalent (e.g., Mg^{2+}, Ca^{2+}) and especially trivalent cations (e.g., Fe^{3+}, Al^{3+}) are much less soluble. Potassium orthophosphates are generally more soluble than the Na orthophosphates and ammonium orthophosphates [24]. In contrast, Ca phosphates are usually poorly soluble or practically insoluble in water. Their solubility decreases in the order $Ca(H_2PO_4)_2$ > $CaHPO_4$ > $Ca_3(PO_4)_2$ > $Ca_5(PO_4)_3OH$ (hydroxyapatite) [23]. The Mg orthophosphates like $MgHPO_4$ and $Mg_3(PO_4)_2$ are more soluble than their Ca analogs, but remain sparingly soluble under neutral conditions and dissolve readily in (dilute) acids [23].

Orthophosphate ions can undergo condensation reactions with the elimination of water (typically achieved by heating) to form more complex phosphates. Condensation of two orthophosphate ions yields a pyrophosphate ion ($P_2O_7^{4-}$) in which two orthophosphate tetrahedra share a corner [22]. Pyrophosphoric acid ($H_4P_2O_7$) has four

pKa values of 0.91, 2.10, 6.70, and 9.32 [24], and under neutral conditions exists as a mixture of $H_2P_2O_7^{2-}$ and $HP_2O_7^{3-}$ ions in aqueous solution. Further condensation leads to the formation of polyphosphates, which are linear chains of orthophosphate units with the general formula $P_nO_{(3n+1)}^{(n+2)-}$. As the chain length increases, the average polyphosphate composition approaches $P_nO_{3n}^{n-}$. These long-chain polyphosphates are different from metaphosphates (or cyclophosphates), which are cyclic (ring-shaped) condensed phosphates with the same general formula $P_nO_{3n}^{n-}$. Ultraphosphates are complex, branched polyphosphates that are formed when some PO_4 tetrahedra are connected to three other PO_4 tetrahedra [25].

Condensed phosphates can form both crystalline salts and amorphous glasses with numerous cations [25]. The glassy, amorphous materials are typically formed by rapid cooling of the melts [23]. The repeating P-O-P backbone of polyphosphates is relatively stable to chemical attack under neutral conditions, but undergoes hydrolytic cleavage to form the original orthophosphate building blocks. This hydrolysis rate is greatly accelerated by elevated temperatures or strongly acidic/alkaline conditions [26, 27]. Solubility trends for pyrophosphates follow those of the orthophosphates, and $K_4P_2O_7 > Na_4P_2O_7$. Most Na and K polyphosphates are water-soluble, except for the high-molecular mass crystalline forms [23]. Similarly, amorphous ammonium polyphosphate is highly soluble [28], but crystalline ammonium polyphosphate has a low solubility [29]. In contrast, condensed Ca phosphates (e.g., $Ca_2P_2O_7$, $Ca_5(P_3O_{10})_2$, and Ca metaphosphate) are considered practically insoluble under neutral conditions [23, 30]. The Mg analogs have similar behaviors but are generally more soluble than their Ca counterparts [31, 32].

2.2. Thermal decomposition of pure phosphates

To predict the phosphate species formed during co-pyrolysis with phosphate compounds, the thermal transformations of the pure phosphate compounds need to be understood first. Starting with the simplest orthophosphate, H_3PO_4 condenses upon heating and releases water, first forming $H_4P_2O_7$. As the condensation reaction proceeds, a complex mixture of linear ($H_{n+2}P_nO_{3n+1}$), cyclic ($(HPO_3)_n$), and possibly branched

polyphosphoric acids of different chain lengths are formed [33, 34]. In the absence of any binding cation, these condensed phosphoric acids are amorphous and thus cannot be identified by XRD.

The decomposition of the ammonium orthophosphates has been under much investigation and is complex due to the overlapping steps. During heating, $(NH_4)_2HPO_4$ first decomposes at around 100-150 °C through the loss of ammonia, which results in the formation of $NH_4H_2PO_4$ [35]. The $NH_4H_2PO_4$ then decomposes at approximately 150-350 °C to form $H_4P_2O_7$ through an intermediate ($NH_4H_3P_2O_7$). The $H_4P_2O_7$ ultimately condenses into $(HPO_3)_n$ at >300 °C [36-38].

The thermal stability of Na phosphates increases as the number of hydrogen atoms decreases. The decomposition of NaH_2PO_4 involves dimerization into $Na_2H_2P_2O_7$ (210-225 °C) and polycondensation into Na polyphosphate $(NaPO_3)_n$ at 260-360 °C [39, 40]. Decomposition of Na_2HPO_4 involves dimerization into a different pyrophosphate ($Na_4P_2O_7$) at around 245-345 °C, but no polycondensation takes place [41]. Finally, Na_3PO_4 undergoes several phase transformations up to 600 °C without weight loss [42].

The least stable of the K orthophosphates, KH_2PO_4, thermally decomposes at around 200-340 °C to form K polyphosphate ($(KPO3)_n$) via a pyrophosphate intermediate ($K_2H_2P_2O_7$) at 260-280 °C [43, 44]. The $(KPO3)_n$ can further undergo phase transformations at 510 and 670 °C and melts at 810 °C [22]. The K_2HPO_4 is more stable and its thermal decomposition takes place at around 280-400 °C to form $K_4P_2O_7$ [45]. If mixtures of KH_2PO_4 and K_2HPO_4 are heated, other intermediates ($K_3HP_2O_7$, $K_5P_3O_{10}$) are formed before finally forming $(KPO_3)_n$ or $K_4P_2O_7$ [45]. The most stable K orthophosphate, K_3PO_4, does not decompose under typical pyrolysis conditions but undergoes a polymorphic transition at around 530 °C [46].

The thermal decomposition of $Mg(H_2PO_4)_2$ is complex and sensitive to environmental conditions [47, 48]. Typically, anhydrous $Mg(H_2PO_4)_2$ condenses and forms $MgH_2P_2O_7$ in the range of 250-380 °C, which is followed by condensation to Mg polyphosphate $(Mg(PO_3)_2)_n$ at around 400-520 °C [47-49]. Upon thermal treatment, $MgHPO_4$ first dehydrates at 120-170 °C to form an amorphous Mg phosphate phase [50, 51]. This amorphous phase is a complex mixture of orthophosphate with polyphosphates of different chain lengths [52]. Upon further

heating, crystalline $Mg_2P_2O_7$ is formed at around 420-600 °C. At higher temperatures, some $Mg_3(PO_4)_2$ may also be formed [50, 53]. This $Mg_3(PO_4)_2$ is stable and does not decompose until well above 1000 °C [13].

During its thermal decomposition, $Ca(H_2PO_4)_2$ condenses and forms $CaH_2P_2O_7$ at around 180-280 °C, which is transformed into Ca metaphosphate $(Ca(PO_3)_2)_n$ at around 280-500 °C [13, 47, 54]. Slow cooling of the metaphosphate promotes the formation of the crystalline form, and rapid quenching is required to obtain an amorphous, glassy form [55]. Upon heating, $CaHPO_4$ dehydrates at around 80-220 °C, resulting in a mixture of poorly crystalline anhydrous $CaHPO_4$ and an amorphous Ca phosphate phase [56, 57]. This mixture further converts into crystalline $Ca_2P_2O_7$ at around 350–550 °C, with phase transformation to a more stable polymorph at >600 °C [52, 54, 56, 57]. Tricalcium phosphate ($Ca_3(PO_4)_2$) has high thermal stability and does not decompose under pyrolysis-relevant conditions [13].

Figure 1 provides an overview of the thermal transformation pathways and approximate stability ranges of the phosphates based on these thermal decomposition mechanisms. Understanding these pathways can aid in the prediction of the dominant phosphate species that will be formed with the selected additive and co-pyrolysis conditions. For example, thermal treatment of tribasic orthophosphates (e.g., Na_3PO_4, K_3PO_4, $Mg_3(PO_4)_2$, $Ca_3(PO_4)_2$) preserves the orthophosphate form, even at high temperatures. In contrast, using protonated phosphates (e.g., KH_2PO_4, K_2HPO_4, $Mg(H_2PO_4)_2$, $MgHPO_4$, and similar) promotes condensation to form of pyro- and/or polyphosphates. Since each of these phosphate forms has its specific properties, their release and plant availability in the P-modified biochars are directly linked to the phosphate form. However, the interaction between these phosphate species and the biomass/biochar components needs to be taken into account as well, as discussed in the next section.

3. Phosphorus transformations during co-pyrolysis with phosphate additives

3.1. Co-pyrolysis with phosphoric acid

Due to its catalytic and dehydrating properties, H_3PO_4 is a common pre-pyrolysis treatment agent for producing porous activated carbon from biomass [58]. The biomass is impregnated with a high concentration of H_3PO_4, which enhances pore formation and increases carbon retention by the formation of thermally stable C-O-P bonds [59, 60]. Because the primary purpose of the H_3PO_4 treatment is to create a porous structure rather than P enrichment, any residual P compounds are typically removed by washing steps and only a small amount of P remains in the solid in the form of phosphate functional groups on the carbon surface [59, 61]. Recently, H_3PO_4 has also been used for P enrichment of feedstocks such as poultry waste [62, 63], sugarcane leaves [64], wheat straw [9], and peanut shells [65] with a H_3PO_4 solution. In this context, the washing step is skipped to ensure maximum P loading.

Examples of biochar modifications by co-pyrolysis with H_3PO_4 are shown in Table 1. Since H_3PO_4 is commercially available in solution form, mixing of H_3PO_4 with the biomass has been done exclusively in wet form. High H_3PO_4:biomass ratios increase the biochar yield and P content [9, 60], although a smaller or no effect is seen at lower H_3PO_4 loadings [62, 64]. The biochars produced by modification with H_3PO_4 typically exhibit a low pH (1.5-2.2) due to the presence of acidic phosphate species. When a low concentration of H_3PO_4 was applied to a high-ash biomass like poultry manure, Sahin et al. [62] reported a much higher pH of 8.57.

The crystalline phases after modification with H_3PO_4 depend on the cations present in the raw material and thus on the biomass composition. For example, biochar from H_3PO_4-modified poultry manure (a Ca-rich feedstock) contained crystalline Ca and Mg phosphates [63], whereas no crystalline phase was found when sugarcane leaves were used as biomass [64].

3.2. Co-pyrolysis with ammonium phosphates

Both $NH_4H_2PO_4$ and $(NH_4)_2HPO_4$ have been used for their fire-retardant properties and their ability to increase char yield [66, 67] by increasing the activation energy for thermal degradation of biomass [68]. More recently, $NH_4H_2PO_4$ and $(NH_4)_2HPO_4$ have been used as co-pyrolysis agents to produce P-enriched biochars for fertilizer application. This application is more effective at retaining P than N, because the P is retained in the char

whereas most of the N is lost to the gas phase during pyrolysis. For example, Suwanree et al. [64] reported that pre-treatment of sugarcane leaves with $(NH_4)_2HPO_4$ and pyrolysis at 600 °C increased the P content from 7 to 81 g/kg, whereas the N content increased from 10 to only 33 g/kg.

Table 2 gives an overview of selected studies that have used ammonium phosphates in co-pyrolysis. Both wet and dry mixing have been carried out. Dry mixing avoids the need for an additional drying step, but may result in lower material homogeneity in the biomass mixture and less effective penetration of P into the biomass pores. Furthermore, particle segregation can occur if the P compound and biomass have different particle sizes, potentially leading to an inhomogeneous product. Wet mixing, on the other hand, allows for a more even distribution and better impregnation of the P compound throughout the biomass due to superior contact. However, this method requires an extra time- and energy-intensive drying step prior to pyrolysis [58]. Overall, the outcomes of the pyrolysis process, such as an increase in the biochar yield and P loading, are similar to those with H_3PO_4.

Similar to H_3PO_4, the final decomposition products of $(NH_4)_2HPO_4$ and $NH_4H_2PO_4$ are XRD-amorphous [37, 40] and acidic (biochars have a pH around 2.0-2.8). Any crystalline phosphates found in the biochars originate from reactions between the phosphate acids and native mineral cations present in the biomass. For example, co-pyrolysis with $NH_4H_2PO_4$ resulted in the formation of struvite-K ($KMgPO_4 \cdot 6H_2O$) in poultry litter biochar (500 °C) [63], KH_2PO_4 in corn stalk biochar (300-700 °C) [69], and KH_2PO_4 and $Ca(PO_3)_2$ in maize straw biochar (650 °C) [70]. Similarly, crystalline $(KPO_3)_n$ was formed when $NH_4H_2PO_4$ was co-pyrolyzed with wheat straw at 550 °C, but not with pine wood [40], which highlights the influence of feedstock composition. No crystalline phosphates were found when sugarcane leaves were co-pyrolyzed with $(NH_4)_2HPO_4$ at 600 °C [64].

Ammonium polyphosphate has also been used as a co-pyrolysis agent. In the study by Huang et al. [65] using peanut shells pyrolyzed at 500 °C for 2 h, co-pyrolysis with H_3PO_4 or ammonium polyphosphate produced higher surface area (201 m^2/g) than $NH_4H_2PO_4$ (100 m^2/g). All phosphate phases were XRD-amorphous (Figure 2a). The solution ^{31}P NMR analysis indicated that ammonium polyphosphate generated relatively more orthophosphate groups, while H_3PO_4 and $NH_4H_2PO_4$ resulted in more pyrophosphate (although orthophosphate was still the main phase observed) (Figure 2b) [65]. This suggests that ammonium polyphosphate was thermally

fragmented into shorter chains [71], whereas H_3PO_4 and $NH_4H_2PO_4$ underwent condensation (according to their thermal decomposition pathways, Section 2.3). This condensation is in agreement with pyrolysis of wheat straw and pine wood with $NH_4H_2PO_4$ at 550 °C, which showed dominant H_3PO_4 peaks at 0.8 ppm and smaller $H_4P_2O_7$ peaks at -11 ppm (Figure 2c) [40].

3.3. Co-pyrolysis with sodium phosphates

Sodium phosphates are not typically used for biochar fertilizer applications because high levels of Na are toxic to plants [72]. Instead, NaH_2PO_4 and Na_2HPO_4 have been added to study their effects on biochar yield and properties. Zhang et al. [40] identified crystalline $(NaPO_3)_3$ and KPO_3 in biochars produced by co-pyrolysis of NaH_2PO_4 with either pine wood or wood straw at 550 °C, which was supported by solid-state ^{31}P NMR analysis (Figure 3). The presence of KPO_3 was ascribed to the reaction of potassium species in the biomass with the phosphorus in NaH_2PO_4.

3.4. Co-pyrolysis with potassium phosphates

Selected studies on co-pyrolysis of biomasses with K phosphates are summarized in Table 3. Modification has primarily been done by wet mixing, with only one study reporting dry mixing at varying KH_2PO_4 concentrations [73]. The resulting biochars are typically alkaline (pH 7-10), with the biochar pH increasing with the K:P ratio of the K phosphate used [69, 74, 75]. Compared to Ca and ammonium phosphates, the increases in biochar yield and P content obtained with K phosphates tend to be slightly lower [69], although the starting K phosphate plays a significant role. For instance, co-pyrolysis of apple tree branches with KH_2PO_4 resulted in the highest biochar yield (50%) compared to K_2HPO_4 and K_3PO_4 (both 40%). On the other hand, K_3PO_4 yielded the highest P content (82 mg/g compared to 42-43 mg/g for KH_2PO_4 and K_2HPO_4) [75]. Similarly, a study with peanut shells found that higher KH_2PO_4 concentrations resulted in higher biochar yields, though the total P content was not reported [73].

The final form of the K phosphate in the biochar depends on the specific starting compound, pyrolysis conditions, and interactions with biomass cations. For example, when corn stalk was pyrolyzed with KH_2PO_4,

Bai et al. [69] identified both KH_2PO_4 and KPO_3 at 300 °C but only KPO_3 at 500 and 700 °C. In co-pyrolysis with K_3PO_4, the original K_3PO_4 has been identified at temperatures ranging from 350 to 950 °C [74, 76], though the formation of K_2HPO_4 (at 450-550 °C) [74] and $K_4P_2O_7$ (at 400-950 °C) [74, 77] has also been reported. Additionally, phosphates often interact with cations like Ca^{2+}, Mg^{2+}, and Al^{3+} in the biomass to form other phosphates. At 500 °C, co-pyrolysis of corn stalk with K_2HPO_4 resulted in K_2HPO_4 and $(Ca/Mg)_3(PO_4)_2$ [78]. Similarly, microwave pyrolysis of cotton stalk with K_3PO_4 led to the formation of K_3PO_4, $Mg_2P_2O_7$, and $Mg_3(PO_4)_2$ due to the interaction with native Mg in the biomass [79]. In co-pyrolysis of sewage sludge, various K-, Mg-, Al-, and Ca-containing phosphates were formed at 500 and 700 °C, but no crystalline phosphates were observed at 300 °C [77]. In line with this, co-pyrolysis of apple tree branches with KH_2PO_4, K_2HPO_4, and K_3PO_4 produced a mixture of various K- and/or Ca-containing ortho- and pyrophosphates [75].

Figure 4 presents the FTIR and solution-state ^{31}P NMR spectra of these biochars. The FTIR spectra (Figure 4a) for all three modified biochars presented new peaks for orthophosphate (538 cm^{-1}) and pyrophosphate vibrations (1152, 1090, and 1027 cm^{-1}). Furthermore, material BC-1 (modified with KH_2PO_4) exhibited peaks at 1290 and 868 cm^{-1} ascribed to metaphosphate (PO_3^-) vibrations. Consistent with the FTIR data, solution-state ^{31}P NMR analysis confirmed that metaphosphate was present in BC-1 but not in the other biochars (Figure 4b) [75]. These observations align with the thermal decomposition pathway of the pure K phosphates, where $(KPO_3)_n$ is formed with KH_2PO_4 but not with K_2HPO_4 and K_3PO_4 (Section 2.3).

3.5. Co-pyrolysis with magnesium phosphates

To the best of our knowledge, the direct co-pyrolysis of biomasses with a defined Mg phosphate has not been reported; instead, P and Mg compounds are commonly added separately. Typical P sources include H_3PO_4 (most commonly), $NH_4H_2PO_4$, $(NH_4)_2HPO_4$, and $Ca(H_2PO_4)_2$, which are then combined with MgO or $MgCl_2$ (Table 4). This approach has been extensively explored for applications as slow release fertilizer and as adsorbent for heavy metals like Cd(II) and Pb(II).

Compared to H_3PO_4 alone, incorporating MgO during pre-treatment shows varying effects on biochar properties. As shown in Table 4, the addition of MgO may increase the yield for some feedstocks, have a negligible effect for others, or even decrease yield, as observed with poultry litter. Similarly, while co-pyrolysis with H_3PO_4 and MgO generally increases the total P content in biochar from sugarcane leaves [64] and coffee husk [60], this was not the case for poultry litter, where the total P content was higher with H_3PO_4 alone [60]. Other studies indicate that increasing the Mg:P ratio in the pre-treatment can lead to a lower biochar yield [11, 80] and higher total P content for sugarcane filter cake [80] but not for sugarcane leaves [11] (Figure 5a). The resulting biochars are typically neutral to slightly acidic, but their pH depends strongly on the feedstock and the Mg:P ratio. Specifically, low Mg:P ratios result in acidic biochars due to excess phosphate, whereas high Mg:P ratios produce alkaline biochars due to excess MgO [11].

When H_3PO_4 and MgO are mixed in the pre-treatment process, a $MgHPO_4$ intermediate is formed [31, 81], which decomposes during pyrolysis to $Mg_2P_2O_7$ and possibly $Mg_3(PO_4)_2$, as outlined in Section 2.3. Indeed, XRD measurements confirmed that $Mg_2P_2O_7$ was the dominant crystalline phase at 400-700 °C in biochars modified with MgO and H_3PO_4, regardless of whether the feedstock was spent green tea leaves (Figure 5b) [81], sugarcane leaves (Figure 5c) [11], sugarcane filter cake [31], or poultry litter [63]. A small amount of $Mg_3(PO_4)_2$ was formed after pyrolysis at 700 °C with spent green tea leaves [81] (see MPTB-7 in Figure 5b) or when wheat straw was pyrolyzed with KH_2PO_4 and $MgCl_2$ at 600 °C [82]. In contrast, low temperature pyrolysis (300 °C) of spent green tea leaves with MgO and H_3PO_4 yielded no crystalline P forms, confirming the presence of amorphous phosphates (see MPTB-3 in Figure 5b) [81].

The Mg:P ratio in the pre-treatment strongly influences the phosphate speciation. For example, when sugarcane filter cake was co-pyrolyzed at 600 °C, $Mg_2P_2O_7$ was the only crystalline P phase at Mg:P ratios of 0.5-1.5; however, with excess Mg (Mg:P = 2) no crystalline phosphate phase was detected, suggesting the formation of amorphous phosphates (Figure 5c) [80]. In contrast, for sugarcane leaves, crystalline $Mg_2P_2O_7$ was found across wider Mg:P ratios (0.5-2), with the highest peak intensity at Mg:P = 0.75 (Figure 5c) [11]. Similarly, microwave pyrolysis of cotton stalk with K_3PO_4 and MgO (Mg:P = 0.25 and 0.5) produced new crystalline peaks

for $MgHPO_4$ and increased XRD peak intensities for $Mg_3(PO_4)_2$ and $Mg_2P_2O_7$ compared to the MgO-free biochar [79]. Surface analysis via XPS provides complementary insights into these P species. For instance, the P 2p signal of a modified sugarcane leaf biochar (1MgP-BC) presented two sets of doublets; a lower energy doublet (134.6 / 133.7 eV) assigned to either orthophosphate or pyrophosphate groups, and a higher energy doublet (136.4 / 135.5 eV) assigned to metaphosphate (Figure 5d) [64].

Finally, the addition of MgO significantly alters the porous properties of the biochar, with the effect being feedstock-dependent. The MgO addition led to a decrease in specific surface area for sugarcane leaves [11, 64], but an increase for poultry litter and coffee husk [60]. When comparing phosphate precursors in poultry litter biochars, combining MgO with $NH_4H_2PO_4$ or $Ca(H_2PO_4)_2$ resulted in a higher specific surface area and greater mesoporosity. In contrast, combining MgO with H_3PO_4 did not affect the specific surface area and only slightly increased the pore volume [83].

3.6. Co-pyrolysis with calcium phosphates

Calcium phosphates, particularly $Ca(H_2PO_4)_2$, have been added in biomass pyrolysis for various reasons, including increasing carbon retention and stabilization, improving fertilizer value, immobilizing or adsorbing heavy metals, and for fuel applications (Table 5). Incorporating $Ca(H_2PO_4)_2$ into the pyrolysis process increased both biochar yield and P content. The resulting biochar tends to be acidic to neutral, with pH values ranging from 3.6 to 7.0 depending on the biomass and pyrolysis conditions.

Typically, the specific Ca phosphate phase formed depends on the modifiers and the Ca:P ratio. For instance, while $Ca(H_2PO_4)_2$-based biochars (with a Ca:P ratio of 0.5) tend to contain $(Ca(PO_3)_2)_n$, separate addition of H_3PO_4 and CaO (equimolar Ca:P ratio) to sugarcane filter cake at 600 °C resulted in crystalline $Ca_2P_2O_7$ as the main phase [31]. This is consistent with the thermal degradation pathway of the $CaHPO_4$ intermediate (Section 2.3). However, when $Ca(H_2PO_4)_2$ is co-pyrolyzed with biomass, the interaction with inherent cations (like K^+) can also lead to the formation of various other phosphate species. For example, in addition to Ca phosphates like $Ca_2P_2O_7$ (at 300-700 °C), $Ca(PO_3)_2$ (at 500-700 °C), and/or $Ca_3(PO_4)_2$ (at 500 °C)

[20, 40, 63, 69, 70, 84], crystalline K-containing phosphates like KPO_3 [40], KH_2PO_4 ([69] $K_5P_3O_{10}$ [63], or mixed phases like $Ca_2KP_3O_{10}$ [69] have been identified.

In the work of Wang et al. [70], co-pyrolysis of maize straw with $Ca(H_2PO_4)_2$ at 650 °C (MSC-CPM) produced $Ca(PO_3)_2$ as the only crystalline P-containing phase (Figure 6a), consistent with its thermal degradation pathway (Section 2.3). In contrast, co-pyrolysis with $NH_4H_2PO_4$ (MSC-ADP) yielded KH_2PO_4, while the unmodified biochar (MSC) did not contain any crystalline P phases (Figure 6a) [70]. Furthermore, when wheat straw was pyrolyzed with $Ca(H_2PO_4)_2$ at 550 °C, XRD analysis confirmed the presence of crystalline $Ca(PO_3)_2$ and KPO_3 (Figure 3a), whereas the solid-state ^{31}P NMR analysis identified a mixture of $Ca_2P_2O_7$, $Ca(PO_3)_2$ and $Ca_3(PO_4)_2$ (Figure 6c). By comparison, pine wood biochar exhibited a simpler ^{31}P NMR spectrum with only $Ca_2P_2O_7$, highlighting the influence of the feedstock on P speciation [40]. Finally, XPS analysis of sawdust co-pyrolyzed with $Ca(H_2PO_4)_2$ (BC_{saw}-TSP) revealed a P 2p spectrum with a higher binding energy (134.4 eV) than either unmodified (BC_{saw}) or bone meal co-pyrolyzed biochars (BC_{saw}-BM) (133.3 eV, Figure 6b). This shift to higher binding energy was ascribed to the formation of C-O-P bonds between the phosphate and the carbonaceous biochar matrix [20].

4. Phosphorus solubility, release, and plant uptake

4.1. Extractable P from phosphorus-modified biochars

The extractability of P-modified biochars has been widely studied, most commonly using deionized (DI) water extraction. Consistent with the behavior of the pure compounds, biochars modified with P sources containing monovalent cations (e.g., H^+, NH_4^+, and K^+) exhibit high levels of water-soluble P, typically accounting for 50-90% of the total P content [64, 79]. An exception to this is when poultry manure was modified with H_3PO_4 and pyrolyzed at 300 °C, where water-soluble P was only 0.1 g/kg (<1% of total P). This was likely due to the comparatively low H_3PO_4 loading used (see Table 1) and the reactions between the acid and the intrinsic divalent cations in the manure [62]. Similarly, co-pyrolysis of H_3PO_4 with divalent metal oxides (MgO or CaO) reduced the water-soluble P levels to <5% of total P [31, 64, 80, 81, 85]. Slightly higher values were found when

MgO was combined with monovalent sources such as $(NH_4)_2HPO_4$ (16% soluble P) [64] and K_3PO_4 (22-48% soluble P) [79]. For Mg/P-modified biochars the low water solubility appears insensitive to process parameters such as the pyrolysis temperature [81] or Mg:P ratio [80]. From an environmental perspective, a lower water-soluble P concentration is critical, as this highly mobile fraction contributes to P losses via surface water runoff [86].

When stronger extractants are used, P extractability significantly increases compared to DI water. For biochars produced with H_3PO_4 and ammonium phosphates, the extractability in 2% formic acid is high, similar to DI water [64]. However, for Mg/P-modified biochars, the extractability in formic acid is significantly higher than in DI water and (unlike in DI water) sensitive to synthesis conditions. Specifically, higher Mg:P ratios and lower pyrolysis temperatures lead to a higher extractability in formic acid, suggesting the formation of more acid-soluble phosphates under these conditions [64, 80, 81]. Other media show a similar high extractability: P extractability from Mg/P-modified biochars in 2% citric acid is 73% [85] and increased to 86-91% in neutral ammonium citrate (NAC) [85, 87]. Interestingly, the effect of MgO addition during pyrolysis depends on the P source: MgO addition slightly decreased extractability for H_3PO_4-modified biochars (from 95% to 91%), but increased NAC-extractable P when $Ca(H_2PO_4)_2$ was used (from 47% to 91%). Finally, studies using 0.2 M EDTA have reported a high P extractability (69-80% of total P) irrespective of Mg content or K_3PO_4 loading [79].

To characterize the different P forms in biochars, studies have used a sequential extraction procedure adapted from the Hedley soil fractionation method [88-90]. This procedure separates the P into pools using reagents of increasing strength: DI water (readily water-soluble P), 0.5 M $NaHCO_3$ (labile P that is readily available to plants), 0.1 M NaOH (moderately labile P associated with Al and Fe oxides/hydroxides), and 1 M HCl (stable P bound within acid-soluble minerals such as apatites) [91, 92]. In Mg/P-modified spent green tea leaf biochars, Jantapa et al. [81] found that the stable HCl-P fraction dominated (37-71% of the total extracted P) across temperatures 300-700 °C. Higher pyrolysis temperatures correlated with a transformation from more plant-available into less available P forms (Figure 7a) [81]. In contrast, Liu and Tian [77] observed that adding K_3PO_4 to iron-rich sewage sludge increased labile (H_2O-P and $NaHCO_3$-P) and especially moderately labile (NaOH-P)

fractions while decreasing HCl-P, independent of temperature (300-500 °C, Figure 7b). Similarly, a K_3PO_4-modified rice husk biochar prepared at 500 °C contained H_2O-P as the largest fraction (59%), followed by $NaHCO_3$-P (16%) (Figure 7c) [12]. This highlights a strong functional contrast between phosphate salts: the P sources that form stable phosphates (e.g., with Mg) promote P stabilization into less soluble, long-term available forms, whereas soluble P compounds (like K_3PO_4) enhance labile nutrient levels.

4.2. Phosphorus release kinetics from phosphorus-modified biochars

The kinetic P release in water has been measured for various modified biochars. Most studies dispersed the biochar in water at a concentration of 5 g/L and agitated the suspension for 240 hours (10 days). Dissolved P concentrations were measured at different time intervals using techniques like ICP-OES [60, 63, 69, 93], which quantifies the total released P but does not distinguish between specific P species. Selected results of total P release are summarized in Figure 8a-e.

The P release from biochars modified with monovalent cation phosphates (e.g., H^+, NH_4^+, and K^+) was generally high and reached approximately 60-210 g P/kg biochar after 240 h, which corresponds to ≥54% of the biochar P content (Figure 8a). This release was also relatively fast, with approximately 65-95% of the total P release occurring within the first 24 h. The highest P release was observed for poultry litter biochar modified with H_3PO_4 [63]. This can be attributed primarily to the high water solubility of H_3PO_4 and its thermal decomposition products, the low pH of the resulting biochar, and the high intrinsic P content of the poultry litter compared to plant-based feedstocks. Generally, P release followed the order: $H_3PO_4 > NH_4H_2PO_4 \approx KH_2PO_4$, with no clear dependence on pyrolysis temperature [63, 69]. This rapid and high release suggests that co-pyrolysis with monovalent cation phosphates produces phosphate compounds that are largely water-soluble and loosely bound to the biochar matrix.

Biochars modified with divalent cations (Mg and Ca phosphates) exhibited significantly slower P release kinetics compared to monovalent modifiers. Less than half of the total P content was released after 240 h (generally below 50 g P/kg biochar), with the majority (49-84%) occurring within the first 24 h (Figure 8b,c). A

direct comparison of Mg to Ca phosphates requires careful attention to stoichiometry: modifications with Ca phosphates typically used a Ca:P ratio of 0.5 (due to the stoichiometry of $Ca(H_2PO_4)_2$), whereas most Mg phosphate modifications used a Mg:P ratio of 1.0. Increasing the Ca:P ratio to 1.0 (e.g., for filter cake) drastically reduced the P release to only 2% after 240 h, confirming the P stabilizing effects of higher Ca:P ratios [31]. Beyond stoichiometry, the phosphate salt and feedstock also significantly influenced P release. For example, combining MgO with H_3PO_4 or $NH_4H_2PO_4$ resulted in a higher release than MgO with $Ca(H_2PO_4)_2$, suggesting that MgO can readily displace protons/ammonium but not Ca^{2+} to form slowly releasing phosphates. The P release was also feedstock-dependent and decreased in the order: coffee husk > poultry litter > spent green tea (at the same pyrolysis temperature and equimolar modification with H_3PO_4 and MgO). While coffee husk and spent green tea are similar in their low intrinsic Ca and P content compared to poultry litter, coffee husk biochar modified with H_3PO_4 and MgO released significantly more P (91 g P/kg biochar) than spent green tea biochar, mainly due to the higher P:biomass ratio used during modification (Table 4). Conversely, poultry litter biochars showed a lower P release compared to plant-based feedstocks like corn stalk, likely due to the formation of highly stable Ca compounds like hydroxyapatite. Finally, pyrolysis temperature affected the P release. While the absolute P release from $Ca(H_2PO_4)_2$-modified corn stalk biochars was independent of temperature, lower temperatures yielded a higher percentage of P release. This may imply that low temperature pyrolysis may generate more soluble phosphates, in contrast to high temperature pyrolysis where $Ca(PO_3)_2$ was formed [69].

As shown in Figures 8d and 8e, comparisons of total P release after 240 h (both absolute values and percentages of biochar P content) confirm that the P release from monovalent cationic modifiers was consistently higher than divalent modifiers. Despite different stoichiometries, the P release from Mg phosphate modified biochars (with Mg:P generally at 1.0) was comparable to that of Ca phosphate modified biochars (with Ca:P ratio of 0.5).

The studies discussed above measured only the total P without distinguishing between specific P forms. However, biochars typically contain various phosphate species (such as orthophosphates, pyrophosphates, and polyphosphates), each with different solubilities and crop availabilities. To address this limitation, some

researchers have employed UV-vis spectroscopy with the molybdenum blue method to quantify the 'molybdate reactive phosphorus', which consists (almost) exclusively of orthophosphate [31, 64, 80, 81, 94]. This approach provides direct information on immediately available P and has been primarily applied to Mg phosphate modified biochars (Figure 8f). Orthophosphate release patterns generally followed those observed for total P: release decreased with increasing pyrolysis temperature and higher Mg:P ratios, and was more rapid for $(NH_4)_2HPO_4$ than H_3PO_4 modifications (due to the lower biochar pH) [64]. Feedstock also played a role, with orthophosphate release decreasing in order: sugarcane leaves > sugarcane filter cake > spent green tea (under identical modification conditions). Consistent with total P release trends, Mg phosphate biochars released orthophosphate more rapidly than Ca phosphate biochars at equivalent cation:P ratios [31]. The most rapid P release was observed with K_3PO_4-modified rice husk biochar [12], where orthophosphate release reached 58% of the biochar P content (36 mg/kg) after 24 hours. Equilibrium was reached within just 2 hours due to the formation of readily soluble phosphates during co-pyrolysis with water-soluble K_3PO_4.

To differentiate between phosphate forms with the molybdenum blue method, a digestion or peroxidation step can be added to convert all P into orthophosphate. Some authors have used this approach to distinguish between orthophosphate and total P concentrations in the final 240-h sample (Figure 8g). The difference between these values represents condensed phosphates (i.e., pyrophosphates and polyphosphates). These results demonstrate that while orthophosphate release was the highest for the 300 °C biochar, condensed phosphate release peaked at 500 °C. Consequently, the total P release was highest at 300-500 °C (19-25% of biochar P content) and decreased at higher temperatures [81]. Notably, for Ca phosphate biochars, while orthophosphate dissolution was low, peroxidation barely increased the measured P concentration, confirming the poor solubility of condensed Ca phosphates [31]. This observation indicates that any condensed phosphates formed in Ca phosphate biochars remain largely insoluble and are retained within the biochar, even after 10 days in water.

Relatively few authors have measured P release kinetics in soil. Studies focusing on K_3PO_4-modified cotton straw biochar, prepared by microwave pyrolysis, demonstrated rapid P release: the K_3PO_4-modified biochar released all its P within 12 days in soil [95]. When 10% or 30% bentonite clay was included, this P release

was reduced to 53% (in 12 days) or 82% (in 20 days), respectively. This slow release behavior was ascribed to the formation of stable Ca and Mg phosphates in the presence of bentonite [95]. Similarly, MgO incorporation also inhibited P release. Consistent with the bentonite findings, the MgO-free K_3PO_4-modified biochar released its P rapidly, while incorporation of MgO slowed the P release to only around 32% after 28 days in soil [79]. Characterization using XRD and XPS analysis confirmed the P release mechanism: water-soluble P dissolved first, followed by precipitated P, and organic P showed the slowest release behavior [79].

4.3. Plant studies

The agronomic performance of Mg/P-modified biochars derived from poultry litter and coffee husk has been demonstrated in several plant studies under controlled greenhouse conditions. Such trials have shown that while triple superphosphate produces higher biomass in the first cycles [63, 87], the biochar-based fertilizers resulted in higher cumulative yields over multiple growth seasons [87, 93]. The mechanism behind this long-term performance was ascribed to the formation of stable, water-insoluble pyrophosphates (e.g.,$Mg_2P_2O_7$ and $Ca_2P_2O_7$) that provide a slow and steady release of P and reduced soil fixation [85, 87]. Sequential P extraction and P diffusion measurements confirmed that soils with modified biochars had significantly higher long-term available P pools than triple superphosphate-amended soils [85, 93].

The combined modification of cotton straw with K_3PO_4 and bentonite improved biomass production in pot-grown pepper plants compared to K_3PO_4-modified biochar [95], although no comparison was made with traditional fertilizers. However, not all modifications are effective. For example, pre-pyrolysis modification of poultry manure with a low concentration of H_3PO_4 increased plant P uptake, but did not significantly increase the plant dry weight compared to the unmodified biochar [62].

5. Comparative analysis of P transformations and release mechanisms

The P species and release kinetics in P-modified biochars are largely governed by three key parameters: (i) the properties of the phosphate modifier salt (specifically the cation identity and protonation state), (ii) the pyrolysis temperature, and (iii) the biomass feedstock composition (especially ash content and native cations)

(Figure 9). Generally, both the additive salt and temperature determine the degree of condensation in the biochar: higher temperatures and higher degrees of protonation (i.e., higher H:P ratios) favor the formation of condensed P species. The specific phosphate salt used dictates the resulting P structure: dihydrogen phosphate salts (e.g., KH_2PO_4, $Ca(H_2PO_4)_2$) tend to form condensed phosphates like polyphosphates at sufficiently high temperatures, whereas hydrogen phosphate salts (e.g., K_2HPO_4, $CaHPO_4$) typically produce pyrophosphates, and tribasic phosphate salts (e.g., K_3PO_4, $Ca_3(PO_4)_2$, generally retain their original orthophosphate structure.

The P solubility and release are directly linked to these structural forms and the binding cations. The cation valency is a major determinant of release kinetics: co-pyrolysis with monovalent cations (K^+, Na^+, NH_4^+) typically yields highly soluble phosphates, irrespective of the H:P ratio and pyrolysis temperature. In contrast, divalent systems (Ca^{2+}, Mg^{2+}) present significantly slower phosphate release, which is further suppressed as the cation:P ratio increases (and H:P ratio decreases). Pyrolysis temperature further influences this behavior, with higher pyrolysis temperatures promoting the formation of less soluble species.

Finally, the native mineral content of the biomass can alter these predicted trends. High ash feedstocks rich in competing cations (such as sewage sludge or poultry manure, Table S1 in Supporting Information) can displace protons or monovalent cations during pyrolysis. For example, in Ca-rich poultry manure, the native Ca^{2+} can react with acidic additives (e.g., H_3PO_4) to form Ca phosphates. This interaction effectively shifts the system towards less soluble phosphates, even when highly soluble phosphate salts are used in co-pyrolysis. Together, these factors provide a basis for the rational design of engineered biochars with targeted P release profiles.

6. Challenges and future research directions

Despite the promising agronomic performance of P-modified biochar fertilizers in greenhouse trials, bridging the gap between laboratory synthesis and commercial application requires overcoming several hurdles (Table 6).

1. Advanced characterization

The analysis of P species in biochars has mainly relied on accessible techniques like XRD, FTIR spectroscopy, and SEM-EDX [13]. While these techniques provide complementary information, they have distinct limitations when describing complex matrices like biochars. XRD is restricted to crystalline phases and gives no insight into the amorphous phosphates that are often present in biochars. Similarly, interpretation of FTIR spectra is often challenging due to low specificity and peak overlap from silicate and carbonate vibrations. While SEM-EDX provides the spatial distribution of P and its location with other elements (e.g., with Ca, Mg, or K), it does not provide information on the chemical speciation or bonding of P. More in-depth characterization is particularly necessary for condensed P phases, as these are often amorphous and tend to be overlooked. To identify the local P structure and binding environment, advanced techniques are increasingly necessary. For example, solid-state and solution ^{31}P NMR spectroscopy can quantify and distinguish between different inorganic phosphates (e.g., orthophosphate, pyrophosphate, and polyphosphate), while XPS is useful for probing the surface chemical states of P in biochars. Synchrotron-based X-ray absorption near edge structure (XANES) spectroscopy is highly sensitive to the local environment of P and is particularly useful in distinguishing between different P species in complex mixtures [96]. Although P-edge XANES has been successfully applied to various biochars [97-99], it may not be readily available due to the requirement of synchrotron radiation and complexity of data interpretation. Future research should employ in situ characterization techniques that monitor P transformations within the biochar, particularly focusing on transitions between orthophosphate, condensed phosphates, and crystalline/amorphous structures.

2. Agronomic effectiveness

The link between P species, release kinetics, and plant uptake has only been established in a few studies. Plant responses have been largely limited to biochars modified with Mg phosphates, with two studies on biochars modified with H_3PO_4 and K_3PO_4. Furthermore, research has mostly focused on poultry manure as feedstock, whereas most modifications have been done on lignocellulosic biomasses. Because the physicochemical properties and effects on plant growth can vary significantly across feedstocks [100], biochars from more diverse feedstocks should be studied. Moreover, evaluations should include biochars co-loaded with N, K, and

micronutrients together with P to create more complete fertilizers. It is critical to determine how these nutrients interact within the biochar matrix and how these interactions influence nutrient release kinetics and overall agronomic efficacy. Finally, there is a substantial lack of data from field trials, which are essential to validate the biochar efficacy under realistic agricultural growth conditions, as results from pot trials may not necessarily translate to those obtained in field trials [101, 102].

Furthermore, there is a strong lack of information on the agronomic efficacy of biochars containing long-chain condensed phosphates such as poly- and metaphosphates. While ammonium polyphosphate fertilizers have been recognized for their ability to reduce P fixation in soil [103], the performance of biochars loaded with condensed phosphates is largely unexplored. A recent study demonstrated that biochar enriched with polyphosphate (as $K_5P_3O_{10}$) was significantly more effective than biochar enriched with orthophosphate (as KH_2PO_4) and unmodified biochar in mitigating Cd toxicity and improving plant growth [104]. Similarly, polyphosphates formed during high temperature pyrolysis were found to be resistant to precipitation with Ca^{2+} and could still be utilized by phosphate-solubilizing bacteria [105]. This suggests that condensed phosphates may offer multifunctional benefits by combining sustained nutrient release with metal chelation, which prompts further investigation.

3. Scale-up and economic feasibility

Finally, the transition from laboratory-scale synthesis to large-scale industrial production faces economic and engineering challenges. Although some studies have suggested that the benefits can outweigh production costs [106-108], profitability is highly context-specific [109, 110]. Biochar production cost can vary widely, from a few dollars to several hundred dollars per ton [107, 111, 112]. A critical factor is the P source: while high-purity P chemicals ensure a consistent product, production costs may be very high. Instead, utilizing P-rich waste streams such as bone meal [20] and manure [21] could minimize raw material costs but requires validation of the product performance, given the variability in waste stream composition. Additionally, large-scale production faces engineering challenges related to heat transfer and mixing uniformity. Ultimately, the economic success remains highly sensitive to fluctuations in market values of the end products [106, 107]. Techno-economic analyses must

also account for revenues obtained from co-products (e.g., bio-oil and biogas [106]) and include benefits beyond the direct financial outcomes (e.g., carbon sequestration) to fully capture the value of the biochars.

Acknowledgements: This research did not receive any specific grant from funding agencies in the public, commercial, or not-for-profit sectors.

Conflicts of interest: There are no conflicts of interest to declare.

Data availability: Data sharing is not applicable to this article as no new data were created or analyzed in this study.

References

1. J.H. Urso, L.M. Gilbertson, Atom conversion efficiency: A new sustainability metric applied to nitrogen and phosphorus use in agriculture, ACS Sustainable Chem. Eng. 6 (2018) 4453-4463. https://doi.org/10.1021/acssuschemeng.7b03600
2. J. Zhu, M. Li, M. Whelan, Phosphorus activators contribute to legacy phosphorus availability in agricultural soils: A review, Sci. Total Environ. 612 (2018) 522-537. https://doi.org/10.1016/j.scitotenv.2017.08.095
3. C.E. Nedelciu, K.V. Ragnarsdottir, P. Schlyter, I. Stjernquist, Global phosphorus supply chain dynamics: Assessing regional impact to 2050, Global Food Secur. 26 (2020) 100426. https://doi.org/10.1016/j.gfs.2020.100426
4. D. Jones, A. Deuss, Understanding the resilience of fertiliser markets to shocks: An overview of fertiliser policies, OECD Food, Agriculture and Fisheries Papers No. 208 (2024). https://doi.org/https://doi.org/10.1787/18156797
5. D. Cordell, S. White, Peak phosphorus: Clarifying the key issues of a vigorous debate about long-term phosphorus security, Sustainability 3 (2011) 2027-2049. https://doi.org/10.3390/su3102027
6. L.C.A. Melo, J. Lehmann, J.S.S. Carneiro, M. Camps-Arbestain, Biochar-based fertilizer effects on crop productivity: A meta-analysis, Plant Soil 472 (2022) 45-58. https://doi.org/10.1007/s11104-021-05276-2
7. L. Ye, M. Camps-Arbestain, Q. Shen, J. Lehmann, B. Singh, M. Sabir, Biochar effects on crop yields with and without fertilizer: A meta-analysis of field studies using separate controls, Soil Use Manage. 36 (2020) 2-18. https://doi.org/10.1111/sum.12546
8. S. Joseph, A.L. Cowie, L. Van Zwieten, N. Bolan, A. Budai, W. Buss, M.L. Cayuela, E.R. Graber, J.A. Ippolito, Y. Kuzyakov, Y. Luo, Y.S. Ok, K.N. Palansooriya, J. Shepherd, S. Stephens, Z. Weng, J. Lehmann, How biochar works, and when it doesn't: A review of mechanisms controlling soil and plant responses to biochar, GCB Bioenergy 13 (2021) 1731-1764. https://doi.org/10.1111/gcbb.12885
9. L. Zhao, X. Cao, W. Zheng, Y. Kan, Phosphorus-assisted biomass thermal conversion: Reducing carbon loss and improving biochar stability, PLoS One 9 (2014) e115373. https://doi.org/10.1371/journal.pone.0115373

10. W. Gu, J. Guo, J. Bai, B. Dong, J. Hu, X. Zhuang, C. Zhang, K. Shih, Co-pyrolysis of sewage sludge and $Ca(H_2PO_4)_2$: heavy metal stabilization, mechanism, and toxic leaching, J. Environ. Manage. 305 (2022) 114292. https://doi.org/10.1016/j.jenvman.2021.114292
11. S. Suwanree, K. Jetsrisuparb, P. Kasemsiri, P. Tharamas, H. Uyama, S. Kuboon, J.T.N. Knijnenburg, Influence of magnesium content and phosphoric acid treatment on cadmium adsorption onto sugarcane leaf biochar, Res. Chem. Intermed. 50 (2024) 3981-4001. https://doi.org/10.1007/s11164-024-05329-y
12. Y. Wu, H. Li, T. Ma, X. Gao, Y. Wu, T. Zhang, Performance and mechanism of lead and cadmium stabilization in soil via two types of phosphorus-enriched biochars, Biocatal. Agric. Biotechnol. 66 (2025) 103588. https://doi.org/10.1016/j.bcab.2025.103588
13. E.O. Lidman Olsson, P. Glarborg, K. Dam-Johansen, H. Wu, Review of phosphorus chemistry in the thermal conversion of biomass: progress and perspectives, Energy Fuels 37 (2023) 6907-6998. https://doi.org/10.1021/acs.energyfuels.2c04048
14. R. Huang, C. Fang, X. Lu, R. Jiang, Y. Tang, Transformation of phosphorus during (hydro)thermal treatments of solid biowastes: reaction mechanisms and implications for P reclamation and recycling, Environ. Sci. Technol. 51 (2017) 10284-10298. https://doi.org/10.1021/acs.est.7b02011
15. J.T.N. Knijnenburg, S. Suwanree, D. Macquarrie, P. Kasemsiri, K. Jetsrisuparb, Phosphorus recovery from animal manures through pyrolysis: phosphorus transformations, release mechanisms, and applications of manure biochars in agriculture, RSC Sustainability 3 (2025) 1084-1101. https://doi.org/10.1039/d4su00524d
16. S.B. Tiwari, W.P. Chan, A. Veksha, G. Lisak, T.T. Lim, Advancing insights into phosphorus transformation during thermochemical treatment of sewage sludge, J. Environ. Manage. 391 (2025) 126505. https://doi.org/10.1016/j.jenvman.2025.126505
17. A. Tumbure, P. Bishop, M. Bretherton, M. Hedley, Co-pyrolysis of maize stover and igneous phosphate rock to produce potential biochar-based phosphate fertilizer with improved carbon retention and liming value, ACS Sustainable Chem. Eng. 8 (2020) 4178-4184. https://doi.org/10.1021/acssuschemeng.9b06958
18. F. Yang, J. Lv, Y. Zhou, S. Wu, J. Sima, Co-pyrolysis of biomass and phosphate tailing to produce potential phosphorus-rich biochar: efficient removal of heavy metals and the underlying mechanisms, Environ. Sci. Pollut. Res. 30 (2023) 17804-17816. https://doi.org/http://doi.org/10.1007/s11356-022-23128-z
19. X. Zhou, D. Xu, Z. Yan, Z. Zhang, X. Wang, Production of new fertilizers by combining distiller's grains waste and wet-process phosphoric acid: Synthesis, characterization, mechanisms and application, J. Cleaner Prod. 367 (2022) 133081. https://doi.org/10.1016/j.jclepro.2022.133081
20. L. Zhao, X. Cao, W. Zheng, J.W. Scott, B.K. Sharma, X. Chen, Copyrolysis of biomass with phosphate fertilizers to improve biochar carbon retention, slow nutrient release, and stabilize heavy metals in soil, ACS Sustainable Chem. Eng. 4 (2016) 1630-1636. https://doi.org/10.1021/acssuschemeng.5b01570
21. J. Qiu, M. Fernandes de Souza, A.A. Robles-Aguilar, S. Ghysels, Y.S. Ok, F. Ronsse, E. Meers, Improving biochar properties by co-pyrolysis of pig manure with bio-invasive weed for use as the soil amendment, Chemosphere 312 (2023) 137229. https://doi.org/10.1016/j.chemosphere.2022.137229
22. D.E.C. Corbridge (1974) The structural chemistry of phosphorus. Elsevier, Amsterdam.
23. S. Havelange, N. Van Lierde, A. Germeau, E. Martins, T. Theys, M. Sonveaux, C. Toussaint, K. Schrödter, G. Bettermann, T. Staffel, Phosphoric acid and phosphates, Ullmann's Encyclopedia of Industrial Chemistry (2000) 1-55. https://doi.org/https://doi.org/10.1002/14356007.a19_465.pub4

24. W.M. Haynes, D.R. Lide, T.J. Bruno (2014) CRC Handbook of Chemistry and Physics. 95th ed. CRC Press, Taylor & Francis Group, Boca Raton, FL.
25. A. Durif (2013) Crystal chemistry of condensed phosphates. Springer Science & Business Media, New York.
26. J.R. Van Wazer (1958) Phosphorus and its compounds. Volume I: Chemistry. Interscience Publishers, Inc., New York.
27. T.M. McBeath, E. Lombi, M.J. McLaughlin, E.K. Bünemann, Polyphosphate-fertilizer solution stability with time, temperature, and pH, J. Plant Nutr. Soil Sci. 170 (2007) 387-391. https://doi.org/10.1002/jpln.200625166
28. B. Wang, Z. Lv, M. Yu, X. Liu, C. Li, Q. Hua, Y. Liu, P. Liu, B. Shen, N. Zhao, J. Ding, J. Tang, One-pot synthesis and hydrolysis behavior of highly water-soluble ammonium polyphosphate, ACS Sustainable Chem. Eng. 10 (2022) 13037-13049. https://doi.org/10.1021/acssuschemeng.2c03169
29. C.Y. Shen, N.E. Stahlheber, D.R. Dyroff, Preparation and characterization of crystalline long-chain ammonium polyphosphates, J. Am. Chem. Soc. 91 (1969) 62-67. https://doi.org/10.1021/ja01029a013
30. E.O. Huffman, J.D. Fleming, Calcium polyphosphate-rate and mechanism of its hydrolytic degradation, J. Phys. Chem. 64 (1960) 240-244. https://doi.org/10.1021/j100831a014
31. K. Jetsrisuparb, T. Jeejaila, C. Saengthip, P. Kasemsiri, Y. Ngernyen, P. Chindaprasirt, J.T.N. Knijnenburg, Tailoring the phosphorus release from biochar-based fertilizers: role of magnesium or calcium addition during co-pyrolysis, RSC Adv. 12 (2022) 30539-30548. https://doi.org/10.1039/d2ra05848k
32. P.A.M. De Bruyne, R.M.H. Verbeeck, F. Verbeek, The solubility of calcium hydrogen phosphate dihydrate and magnesium hydrogen phosphate trihydrate and ion pair formation in the system $M(OH)_2$-H_3PO_4-H_2O (M = Ca or Mg) at 37°C, Bull. Soc. Chim. Belg. 99 (1990) 543-552. https://doi.org/10.1002/bscb.19900990805
33. A.-L. Huhti, P.A. Gartaganis, The composition of the strong phosphoric acids, Can. J. Chem. 34 (1956) 785-797. https://doi.org/https://doi.org/10.1139/v56-102
34. S. Ohashi, H. Sugatani, The composition of strong phosphoric acids, Bull. Chem. Soc. Jpn. 30 (1957) 864-867. https://doi.org/truhttps://doi.org/10.1246/bcsj.30.864
35. M. Maciejewski, R. Rudnicki, Correlation between isothermal and rising temperature experiments. Thermal decomposition of diammonium hydrophosphate, Thermochim. Acta 113 (1987) 305-320. https://doi.org/10.1016/0040-6031(87)88333-8
36. C.A. Trujillo, N.T. Ramírez-Marquez, J.S. Valencia-Rios, An affordable ammonia temperature-programmed desorption equipment and its calibration using the thermal decomposition of ammonium dihydrogen phosphate, Thermochim. Acta 689 (2020) 178651. https://doi.org/10.1016/j.tca.2020.178651
37. A. Abdel-Kader, A.A. Ammar, S.I. Saleh, Thermal behaviour of ammonium dihydrogen phosphate crystals in the temperature range 25-600° C, Thermochim. Acta 176 (1991) 293-304. https://doi.org/10.1016/0040-6031(91)80285-Q
38. A. Pardo, J. Romero, E. Ortiz, High-temperature behaviour of ammonium dihydrogen phosphate, J. Phys.: Conf. Ser. 935 (2017) 012050. https://doi.org/https://doi.org/10.1088/1742-6596/935/1/012050
39. A. Ghule, R. Murugan, H. Chang, Thermo-Raman studies on $NaH_2PO_4 \cdot 2H_2O$ for dehydration, condensation, and phase transformation, Inorg. Chem. 40 (2001) 5917-5923. https://doi.org/10.1021/ic010043w
40. W. Zhang, E.O. Lidman Olsson, K. Enemark-Rasmussen, P. Glarborg, K. Dam-Johansen, S. Li, T. Khazraie, H. Kinnunen, J. Roppo, H. Wu, An experimental study of the transformation of phosphorus additives during biomass pyrolysis, Fuel 398 (2025) 135554. https://doi.org/10.1016/j.fuel.2025.135554
41. A. Ghule, C. Bhongale, H. Chang, Monitoring dehydration and condensation processes of $Na_2HPO_4 \cdot 12H_2O$ using thermo-Raman spectroscopy, Spectrochim. Acta A Mol. Biomol. Spectrosc. 59 (2003) 1529-1539. https://doi.org/10.1016/S1386-1425(02)00395-5

42. A. Ghule, N. Baskaran, R. Murugan, H. Chang, Phase transformation studies of Na_3PO_4 by thermo-Raman and conductivity measurements, Solid State Ionics 161 (2003) 291-299. https://doi.org/10.1016/S0167-2738(03)00128-0
43. T. Vlase, G. Vlase, N. Doca, Kinetics of thermal decomposition of alkaline phosphates, J. Therm. Anal. Calorim. 80 (2005) 207-210. https://doi.org/10.1007/s10973-005-0637-2
44. M.E. Brown, L. Glasser, J. Larson, High temperature thermal properties of KH_2PO_4: Phase transitions and decompositions, Thermochim. Acta 30 (1979) 233-246. https://doi.org/10.1016/0040-6031(79)85057-1
45. R.K. Osterheld, L.F. Audrieth, Polymerization and depolymerization phenomena in phosphate-metaphosphate systems at higher temperatures. Condensation reactions involving the potassium hydrogen orthophosphates, J. Phys. Chem. 56 (1952) 38-42. https://doi.org/10.1021/j150493a009
46. D.N. Mosin, E.A. Marks, E.I. Burmakin, N.G. Molchanova, G.S. Shekhtman, Electroconduction of potassium, rubidium, and cesium orthophosphates, Russ. J. Electrochem. 37 (2001) 863-864. https://doi.org/10.1023/A:1016751506735
47. M. Pyldme, K. Tynsuaadu, F. Paulik, J. Paulik, M. Arnold, Dehydrations of $Ca(H_2PO_4)_2{\cdot}H_2O$ and $Mg(H_2PO_4)_2{\cdot}2H_2O$ and their reactions with KCl, examined with simultaneous TG, DTG, DTA and EGA, J. Therm. Anal. 17 (1979) 479-488. https://doi.org/10.1007/BF01914036
48. V.V. Samuskevich, O.A. Lukyanchenko, Thermal transformations of $Mg(H_2PO_4)_2{\cdot}4H_2O$, Thermochim. Acta 311 (1998) 87-95. https://doi.org/10.1016/s0040-6031(97)00420-6
49. S. Ahmed, Part VII. Study of X-ray powder diffraction, infrared absorption and differential thermal analyses of the compounds $Mg(H_2PO_4)2{\cdot}4H_2O$, $Mg(H_2PO_4)_2{\cdot}2H_2O$, $Mg(H_2PO_4)_2$ and $Mg(PO_3)_2$, Pak. J. Sci. Ind. Res. 15 (1972) 142-145.
50. M.A. Aramendía, V. Borau, C. Jiménez, J.M. Marinas, F.J. Romero, J.R. Ruiz, Characterization by XRD, DRIFT, and MAS NMR spectroscopies of a $Mg_2P_2O_7$ catalyst, J. Colloid Interface Sci. 202 (1998) 456-461. https://doi.org/10.1006/jcis.1998.5465
51. D.J. Sutor, S.E. Wooley, Phase changes during heating of magnesium ammonium phosphate hexahydrate and magnesium hydrogen phosphate trihydrate to high temperatures, J. Chem. Soc. A (1968) 1143-1144. https://doi.org/10.1039/J19680001143
52. B.C. Sales, B.C. Chakoumakos, L.A. Boatner, J.O. Ramey, Structural properties of the amorphous phases produced by heating crystalline $MgHPO_4{\cdot}3H_2O$, J. Non-Cryst. Solids 159 (1993) 121-139. https://doi.org/w
53. M.A. Aramendía, V. Borau, C. Jiménez, J.M. Marinas, F.J. Romero, Synthesis and characterization of magnesium phosphates and their catalytic properties in the conversion of 2-hexanol, J. Colloid Interface Sci. 217 (1999) 288-298. https://doi.org/10.1006/jcis.1999.6380
54. L.K. Lin, J.S. Lee, C.K. Hsu, P.J. Huang, H.T. Lin, A study on the thermal properties of dibasic calcium hydrogen phosphate and monobasic calcium phosphate, Anal. Sci. 13 (1997) 413-418. https://doi.org/10.2116/analsci.13.supplement_413
55. E.H. Brown, J.R. Lehr, Fertilizer materials: Vitreous calcium metaphosphate - some properties of its aqueous systems, J. Agric. Food Chem. 12 (1964) 201-204. https://doi.org/10.1021/jf60133a002
56. A. Dosen, R.F. Giese, Thermal decomposition of brushite, $CaHPO_4{\cdot}2H_2O$ to monetite $CaHPO_4$ and the formation of an amorphous phase, Am. Mineral. 96 (2011) 368-373. https://doi.org/10.2138/am.2011.3544
57. M. El Hazzat, A. El Hamidi, M. Halim, S. Arsalane, Complex evolution of phase during the thermal investigation of Brushite-type calcium phosphate $CaHPO_4{\bullet}2H_2O$, Materialia 16 (2021) 101055. https://doi.org/10.1016/j.mtla.2021.101055
58. Z. Heidarinejad, M.H. Dehghani, M. Heidari, G. Javedan, I. Ali, M. Sillanpää, Methods for preparation and activation of activated carbon: a review, Environ. Chem. Lett. 18 (2020) 393-415. https://doi.org/10.1007/s10311-019-00955-0

59. L. Zhao, W. Zheng, O. Mašek, X. Chen, B. Gu, B.K. Sharma, X. Cao, Roles of phosphoric acid in biochar formation: Synchronously improving carbon retention and sorption capacity, J. Environ. Qual. 46 (2017) 393-401. https://doi.org/10.2134/jeq2016.09.0344
60. J.S.D.S. Carneiro, J.F. Lustosa Filho, B.O. Nardis, J. Ribeiro-Soares, Y.L. Zinn, L.C.A. Melo, Carbon stability of engineered biochar-based phosphate fertilizers, ACS Sustainable Chem. Eng. 6 (2018) 14203-14212. https://doi.org/10.1021/acssuschemeng.8b02841
61. G. Chu, J. Zhao, Y. Huang, D. Zhou, Y. Liu, M. Wu, H. Peng, Q. Zhao, B. Pan, C.E.W. Steinberg, Phosphoric acid pretreatment enhances the specific surface areas of biochars by generation of micropores, Environ. Pollut. 240 (2018) 1-9. https://doi.org/10.1016/j.envpol.2018.04.003
62. O. Sahin, M.B. Taskin, E.C. Kaya, O. Atakol, E. Emir, A. Inal, A. Gunes, Effect of acid modification of biochar on nutrient availability and maize growth in a calcareous soil, Soil Use Manage. 33 (2017) 447-456. https://doi.org/10.1111/sum.12360
63. J.F. Lustosa Filho, E.S. Penido, P.P. Castro, C.A. Silva, L.C.A. Melo, Co-pyrolysis of poultry litter and phosphate and magnesium generates alternative slow-release fertilizer suitable for tropical soils, ACS Sustainable Chem. Eng. 5 (2017) 9043-9052. https://doi.org/10.1021/acssuschemeng.7b01935
64. S. Suwanree, J.T.N. Knijnenburg, P. Kasemsiri, W. Kraithong, P. Chindaprasirt, K. Jetsrisuparb, Engineered biochar from sugarcane leaves with slow phosphorus release kinetics, Biomass Bioener. 156 (2022) 106304. https://doi.org/10.1016/j.biombioe.2021.106304
65. K. Huang, C. Hu, Q. Tan, M. Yu, S. Shabala, L. Yang, X. Sun, Highly efficient removal of cadmium from aqueous solution by ammonium polyphosphate-modified biochar, Chemosphere 305 (2022) 135471. https://doi.org/10.1016/j.chemosphere.2022.135471
66. C. Di Blasi, C. Branca, A. Galgano, Effects of diammonium phosphate on the yields and composition of products from wood pyrolysis, Ind. Eng. Chem. Res. 46 (2007) 430-438. https://doi.org/10.1021/ie0612616
67. H. Li, K. Han, Q. Wang, C. Lu, Pyrolysis of rice straw with ammonium dihydrogen phosphate: Properties and gaseous potassium release characteristics during combustion of the products, Bioresour. Technol. 197 (2015) 193-200. https://doi.org/10.1016/j.biortech.2015.08.070
68. O. Das, A.K. Sarmah, Mechanism of waste biomass pyrolysis: Effect of physical and chemical pre-treatments, Sci. Total Environ. 537 (2015) 323-334. https://doi.org/10.1016/j.scitotenv.2015.07.076
69. T. Bai, W. Ma, W. Li, J. Jiang, J. Chen, R. Cao, W. Yang, D. Dong, T. Liu, Y. Xu, Effect of different phosphates on pyrolysis temperature-dependent carbon sequestration and phosphorus release performance in biochar, Molecules 28 (2023) 3950. https://doi.org/10.3390/molecules28093950
70. Q. Wang, K. Han, P. Wang, Influence of phosphorus-based additives on potassium transformation during pyrolysis and ash characteristics of biochar briquettes, Bioenergy Research 13 (2020) 907-917. https://doi.org/10.1007/s12155-020-10118-7
71. G. Camino, N. Grassie, I.C. McNeill, Influence of the fire retardant, ammonium polyphosphate, on the thermal degradation of poly(methyl methacrylate), J. Polym. Sci. Polym. Chem. Ed. 16 (1978) 95-106. https://doi.org/10.1002/pol.1978.170160110
72. H.J. Kronzucker, D. Coskun, L.M. Schulze, J.R. Wong, D.T. Britto, Sodium as nutrient and toxicant, Plant Soil 369 (2013) 1-23. https://doi.org/10.1007/s11104-013-1801-2
73. Y. Zhang, X. Cheng, Z. Wang, M.H. Tahir, M. Wang, Co-pyrolysis of peanut shell with phosphate fertilizer to improve carbon sequestration and emission reduction potential of biochar, Fuel Process. Technol. 236 (2022) 107435. https://doi.org/10.1016/j.fuproc.2022.107435

74. H. Zhang, W. Liao, X. Zhou, J. Shao, Y. Chen, S. Zhang, H. Chen, Coeffect of pyrolysis temperature and potassium phosphate impregnation on characteristics, stability, and adsorption mechanism of phosphorus-enriched biochar, Bioresour. Technol. 344 (2022) 126273. https://doi.org/10.1016/j.biortech.2021.126273
75. Q. Wang, C.J. Duan, C.Y. Xu, Z.C. Geng, Efficient removal of Cd(II) by phosphate-modified biochars derived from apple tree branches: Processes, mechanisms, and application, Sci. Total Environ. 819 (2022) 152876. https://doi.org/10.1016/j.scitotenv.2021.152876
76. H. Yang, Y. Yu, H. Zhang, W. Wang, J. Zhu, Y. Chen, S. Zhang, H. Chen, Effect mechanism of phosphorous-containing additives on carbon structure evolution and biochar stability enhancement, Biochar 6 (2024) 39. https://doi.org/10.1007/s42773-024-00330-5
77. Q.S. Liu, T. Tian, Co-pyrolysis of iron-rich sewage sludge and potassium phosphate to prepare biochars: P fractionation and alleviated occlusion, J. Anal. Appl. Pyrolysis 159 (2021) 105285. https://doi.org/10.1016/j.jaap.2021.105285
78. H. Sha, J. Li, L. Wang, H. Nong, G. Wang, T. Zeng, Preparation of phosphorus-modified biochar for the immobilization of heavy metals in typical lead-zinc contaminated mining soil: Performance, mechanism and microbial community, Environ. Res. 218 (2023) 114769. https://doi.org/10.1016/j.envres.2022.114769
79. Z. Liu, F. Tian, X. An, Z. Wu, T. Li, Q. Yang, Microwave co-pyrolysis of biomass, phosphorus, and magnesium for the preparation of biochar-based fertilizer: Fast synthesis, regulable structure, and graded-release, J. Environ. Chem. Eng. 9 (2021) 106456. https://doi.org/10.1016/j.jece.2021.106456
80. J.T.N. Knijnenburg, P. Kasemsiri, W. Kaewpradit, T. Tarinta, W. Jantapa, T. Jeejaila, C. Saengthip, K. Jetsrisuparb, Co-pyrolysis of biomass with magnesium and phosphorus: effect of magnesium content on phosphate release from biochar-based fertilizers, Biomass Convers. Biorefin. 14 (2024) 15351–15361. https://doi.org/10.1007/s13399-023-03994-4
81. W. Jantapa, K. Jetsrisuparb, D. Macquarrie, P. Kasemsiri, P. Chindaprasirt, J.T.N. Knijnenburg, Temperature-dependent phosphorus speciation and release from magnesium-rich biochars, Waste Biomass Valorization 16 (2025) 2287-2300. https://doi.org/10.1007/s12649-024-02824-6
82. Q. Miao, G. Li, Potassium phosphate/magnesium oxide modified biochars: Interfacial chemical behaviours and Pb binding performance, Sci. Total Environ. 759 (2021) 143452. https://doi.org/10.1016/j.scitotenv.2020.143452
83. E.S. Penido, L.C.A. Melo, L.R.G. Guilherme, M.L. Bianchi, Cadmium binding mechanisms and adsorption capacity by novel phosphorus/magnesium-engineered biochars, Sci. Total Environ. 671 (2019) 1134-1143. https://doi.org/10.1016/j.scitotenv.2019.03.437
84. Y. Zeng, Y. Lin, M. Ma, H. Chen, Adsorption effect and mechanism of Cd(II) by different phosphorus-enriched biochars, Environ. Sci. Pollut. Res. 31 (2024) 16642-16652. https://doi.org/10.1007/s11356-024-32308-y
85. J.F. Lustosa Filho, C.F. Barbosa, J.S.D.S. Carneiro, L.C.A. Melo, Diffusion and phosphorus solubility of biochar-based fertilizer: Visualization, chemical assessment and availability to plants, Soil Tillage Res. 194 (2019) 104298. https://doi.org/10.1016/j.still.2019.104298
86. P.J.A. Kleinman, A.N. Sharpley, A.M. Wolf, D.B. Beegle, P.A. Moore Jr, Measuring water-extractable phosphorus in manure as an indicator of phosphorus in runoff, Soil Sci. Soc. Am. J. 66 (2002) 2009-2015. https://doi.org/10.2136/sssaj2002.2009
87. J.F. Lustosa Filho, J.S.D.S. Carneiro, C.F. Barbosa, K.P. de Lima, A.D.A. Leite, L.C.A. Melo, Aging of biochar-based fertilizers in soil: Effects on phosphorus pools and availability to Urochloa brizantha grass, Sci. Total Environ. 709 (2020) 136028. https://doi.org/10.1016/j.scitotenv.2019.136028

88. M. Hedley, J. Stewart, B. Chauhan, Changes in inorganic and organic soil phosphorus fractions induced by cultivation practices and by laboratory incubations, Soil Sci. Soc. Am. J. 46 (1982) 970-976. https://doi.org/https://doi.org/10.2136/sssaj1982.03615995004600050017x

89. J.S. Robinson, P. Leinweber, Effects of pyrolysis and incineration on the phosphorus fertiliser potential of bio-waste- and plant-based materials, Waste Manage. 172 (2023) 358-367. https://doi.org/10.1016/j.wasman.2023.10.012

90. G. Xu, Y. Zhang, H. Shao, J. Sun, Pyrolysis temperature affects phosphorus transformation in biochar: Chemical fractionation and ^{31}P NMR analysis, Sci. Total Environ. 569-570 (2016) 65-72. https://doi.org/10.1016/j.scitotenv.2016.06.081

91. S. Buehler, A. Oberson, I.M. Rao, D.K. Friesen, E. Frossard, Sequential phosphorus extraction of a ^{33}P-labeled Oxisol under contrasting agricultural systems, Soil Sci. Soc. Am. J. 66 (2002) 868-877. https://doi.org/10.2136/sssaj2002.8680

92. T.T. Qian, H. Jiang, Migration of phosphorus in sewage sludge during different thermal treatment processes, ACS Sustainable Chem. Eng. 2 (2014) 1411-1419. https://doi.org/10.1021/sc400476j

93. J.S.D.S. Carneiro, I.C.A. Ribeiro, B.O. Nardis, C.F. Barbosa, J.F. Lustosa Filho, L.C.A. Melo, Long-term effect of biochar-based fertilizers application in tropical soil: Agronomic efficiency and phosphorus availability, Sci. Total Environ. 760 (2021) 143955. https://doi.org/10.1016/j.scitotenv.2020.143955

94. E.A. Nagul, I.D. McKelvie, P. Worsfold, S.D. Kolev, The molybdenum blue reaction for the determination of orthophosphate revisited: Opening the black box, Anal. Chim. Acta 890 (2015) 60-82. https://doi.org/10.1016/j.aca.2015.07.030

95. X. An, Z. Wu, J. Yu, G. Cravotto, X. Liu, Q. Li, B. Yu, Copyrolysis of biomass, bentonite, and nutrients as a new strategy for the synthesis of improved biochar-based slow-release fertilizers, ACS Sustainable Chem. Eng. 8 (2020) 3181-3190. https://doi.org/10.1021/acssuschemeng.9b06483

96. A. Tofoni, F. Tavani, I. Persson, P. D'Angelo, P K-edge XANES calculations of mineral standards: Exploring the potential of theoretical methods in the analysis of phosphorus speciation, Inorg. Chem. 62 (2023) 11188-11198. https://doi.org/10.1021/acs.inorgchem.3c01346

97. X. Liang, Y. Jin, M. He, C. Niyungeko, J. Zhang, C. Liu, G. Tian, Y. Arai, Phosphorus speciation and release kinetics of swine manure biochar under various pyrolysis temperatures, Environ. Sci. Pollut. Res. 25 (2018) 25780-25788. https://doi.org/10.1007/s11356-017-0640-8

98. R. Huang, C. Fang, B. Zhang, Y. Tang, Transformations of phosphorus speciation during (hydro)thermal treatments of animal manures, Environ. Sci. Technol. 52 (2018) 3016-3026. https://doi.org/10.1021/acs.est.7b05203

99. J.S. Robinson, K. Baumann, Y. Hu, P. Hagemann, L. Kebelmann, P. Leinweber, Phosphorus transformations in plant-based and bio-waste materials induced by pyrolysis, Ambio 47 (2018) 73-82. https://doi.org/10.1007/s13280-017-0990-y

100. L. Qian, L. Chen, S. Joseph, G. Pan, L. Li, J. Zheng, X. Zhang, J. Zheng, X. Yu, J. Wang, Biochar compound fertilizer as an option to reach high productivity but low carbon intensity in rice agriculture of China, Carbon Manage. 5 (2014) 145-154. https://doi.org/10.1080/17583004.2014.912866

101. V. Vijay, S. Shreedhar, K. Adlak, S. Payyanad, V. Sreedharan, G. Gopi, T. Sophia van der Voort, P. Malarvizhi, S. Yi, J. Gebert, P.V. Aravind, Review of large-scale biochar field-trials for soil amendment and the observed influences on crop yield variations, Front. Energy Res. 9 (2021) 710766. https://doi.org/10.3389/fenrg.2021.710766

102. D. Huygens, H.G.M. Saveyn, Agronomic efficiency of selected phosphorus fertilisers derived from secondary raw materials for European agriculture. A meta-analysis, Agron. Sustain. Dev. 38 (2018) 52. https://doi.org/10.1007/s13593-018-0527-1

103. Y. Gao, X. Wang, J.A. Shah, G. Chu, Polyphosphate fertilizers increased maize (Zea mays L.) P, Fe, Zn, and Mn uptake by decreasing P fixation and mobilizing microelements in calcareous soil, J. Soils Sediments 20 (2020) 1-11. https://doi.org/10.1007/s11368-019-02375-7

104. R. Naciri, M. Chtouki, L. El Maalam, H. Hirt, D. Belkachach, A. Oukarroum, Phosphate-modified biochar attenuates cadmium availability in contaminated soil and reduces its transfer to tomato fruits, Environ. Res. 279 (2025) 121775. https://doi.org/10.1016/j.envres.2025.121775

105. T. Qian, W.S. Ong, D. Lu, Y. Zhou, A potential phosphorus fertilizer to alleviate the coming "phosphorus crisis"-biochar derived from enhanced biological phosphorus removal sludge, Sci. Total Environ. 838 (2022) 156559. https://doi.org/10.1016/j.scitotenv.2022.156559

106. M. O'Boyle, B.A. Mohamed, L.Y. Li, Co-pyrolysis of sewage sludge and biomass waste into biofuels and biochar: A comprehensive feasibility study using a circular economy approach, Chemosphere 350 (2024). https://doi.org/10.1016/j.chemosphere.2023.141074

107. T. Haeldermans, L. Campion, T. Kuppens, K. Vanreppelen, A. Cuypers, S. Schreurs, A comparative techno-economic assessment of biochar production from different residue streams using conventional and microwave pyrolysis, Bioresour. Technol. 318 (2020) 124083. https://doi.org/10.1016/j.biortech.2020.124083

108. U. Pongsa, P. Lumsakul, O. Jamesang, P. Saengkhiao, P. Sangrayub, W. Pumchan, Feasibility study of coconut shell biochar production using community-scale biochar kiln, J. Met., Mater. Miner. 33 (2023) 128-138. https://doi.org/10.55713/jmmm.v33i2.1699

109. D. Dickinson, L. Balduccio, J. Buysse, F. Ronsse, G. van Huylenbroeck, W. Prins, Cost-benefit analysis of using biochar to improve cereals agriculture, GCB Bioenergy 7 (2015) 850-864. https://doi.org/10.1111/gcbb.12180

110. A.E. Latawiec, B.B.N. Strassburg, A.B. Junqueira, E. Araujo, L.F. D. de Moraes, H.A.N. Pinto, A. Castro, M. Rangel, G.A. Malaguti, A.F. Rodrigues, L.G. Barioni, E.H. Novotny, G. Cornelissen, M. Mendes, N. Batista, J.G. Guerra, E. Zonta, C. Jakovac, S.E. Hale, Biochar amendment improves degraded pasturelands in Brazil: environmental and cost-benefit analysis, Sci. Rep. 9 (2019) 11993. https://doi.org/10.1038/s41598-019-47647-x

111. M. Azuara, S.R.A. Kersten, A.M.J. Kootstra, Recycling phosphorus by fast pyrolysis of pig manure: Concentration and extraction of phosphorus combined with formation of value-added pyrolysis products, Biomass Bioener. 49 (2013) 171-180. https://doi.org/10.1016/j.biombioe.2012.12.010

112. E. Struhs, A. Mirkouei, Y. You, A. Mohajeri, Techno-economic and environmental assessments for nutrient-rich biochar production from cattle manure: A case study in Idaho, USA, Appl. Energy 279 (2020) 115782. https://doi.org/https://doi.org/10.1016/j.apenergy.2020.115782

113. A. Ghule, R. Murugan, H. Chang, Thermo-Raman studies on dehydration of $Na_3PO_4 \cdot 12H_2O$, Thermochim. Acta 371 (2001) 127-135. https://doi.org/10.1016/S0040-6031(00)00719-X

114. F. Li, X. Cao, L. Zhao, J. Wang, Z. Ding, Effects of mineral additives on biochar formation: Carbon retention, stability, and properties, Environ. Sci. Technol. 48 (2014) 11211-11217. https://doi.org/10.1021/es501885n

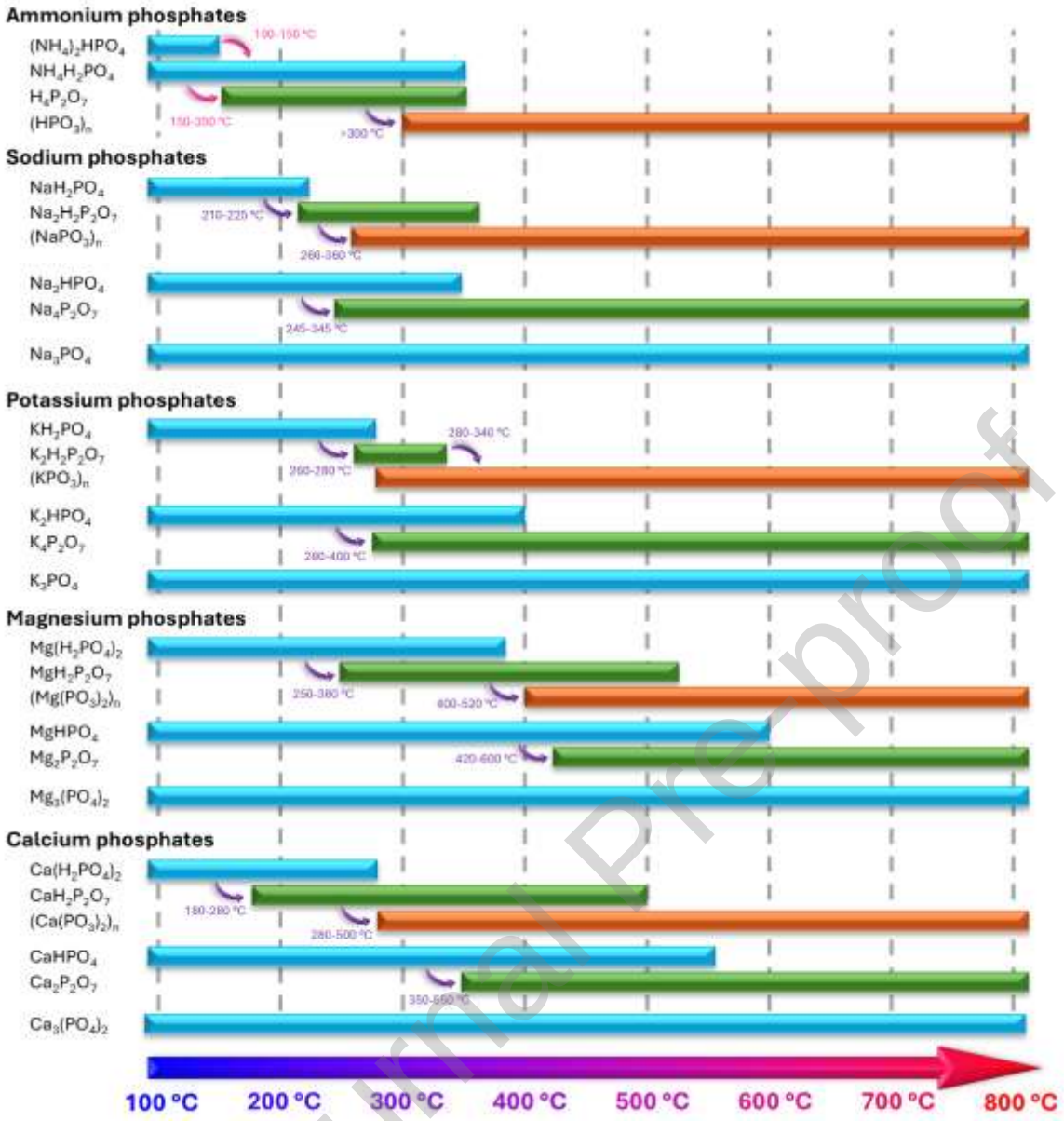

Figure 1. Thermal transformation pathways and stability ranges of selected phosphate compounds based on reported thermochemical data for ammonium phosphates [35-38], sodium phosphates [39-42, 113], potassium phosphates [43-46], magnesium phosphates [47-53], and calcium phosphates [47, 54, 56, 57]. Horizontal bars indicate the temperature ranges over which each dominant phosphate is stable: orthophosphates (blue), pyrophosphates (green), and poly-/metaphosphates (orange). Arrows indicate transformation pathways at the indicated temperature ranges. Purple arrows are condensation reactions (releasing $H_2O(g)$), and pink arrows at the ammonium phosphates denote loss of $NH_3(g)$. The transition temperatures are generalized from literature and may vary depending on specific experimental conditions (e.g., heating rate, gas atmosphere, and sample

size/structure). For clarity, only the anhydrous compounds are shown, and melting/polymorph transitions are omitted.

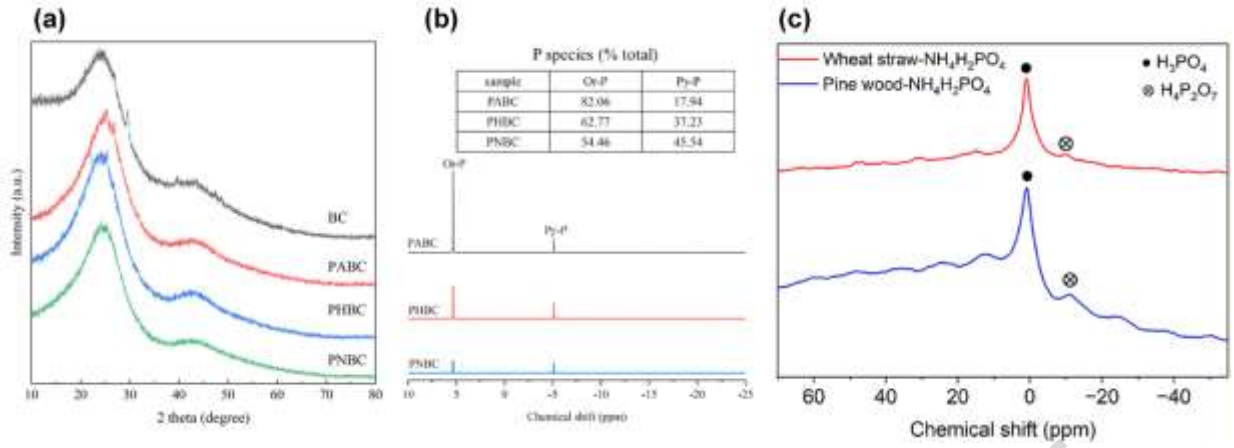

Figure 2. (a) X-ray diffraction patterns and (b) solution-state ^{31}P NMR spectra of the NaOH-EDTA extracts of peanut shell biochars (500 °C) modified with ammonium polyphosphate (PABC), H_3PO_4 (PHBC), and $NH_4H_2PO_4$ (PNBC) compared to the unmodified biochar (BC). Reprinted (adapted) from Huang et al. [65] with permission from Elsevier, 2022; (c) solid-state ^{31}P NMR spectra of $NH_4H_2PO_4$-modified wheat straw and pine wood biochars produced at 550 °C. Reprinted (adapted) from Zhang et al. [40] under the Creative Commons Attribution (CC BY) license.

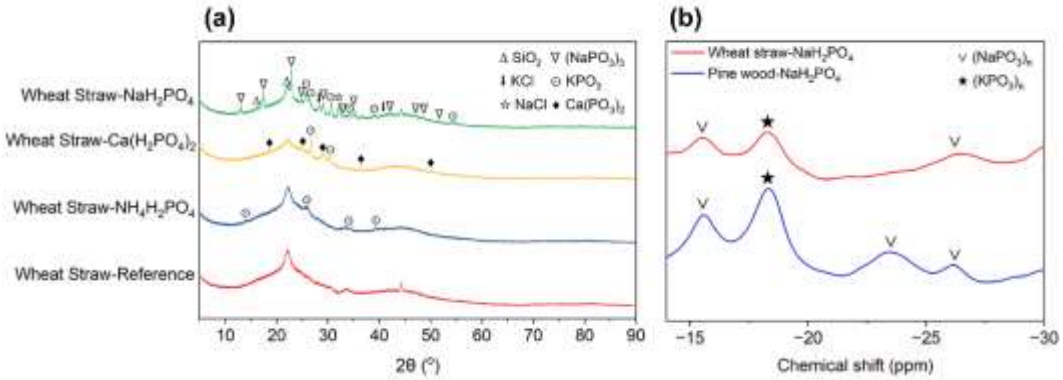

Figure 3. (a) X-ray diffraction patterns of wheat straw biochars produced at 550 °C modified with NaH_2PO_4, $Ca(H_2PO_4)_2$, and $NH_4H_2PO_4$ compared to the unmodified biochars; (b) solid-state ^{31}P NMR spectra of wheat straw and pine wood biochars modified with NaH_2PO_4 produced at 550 °C. Reprinted (adapted) from Zhang et al. [40] under the Creative Commons Attribution (CC BY) license.

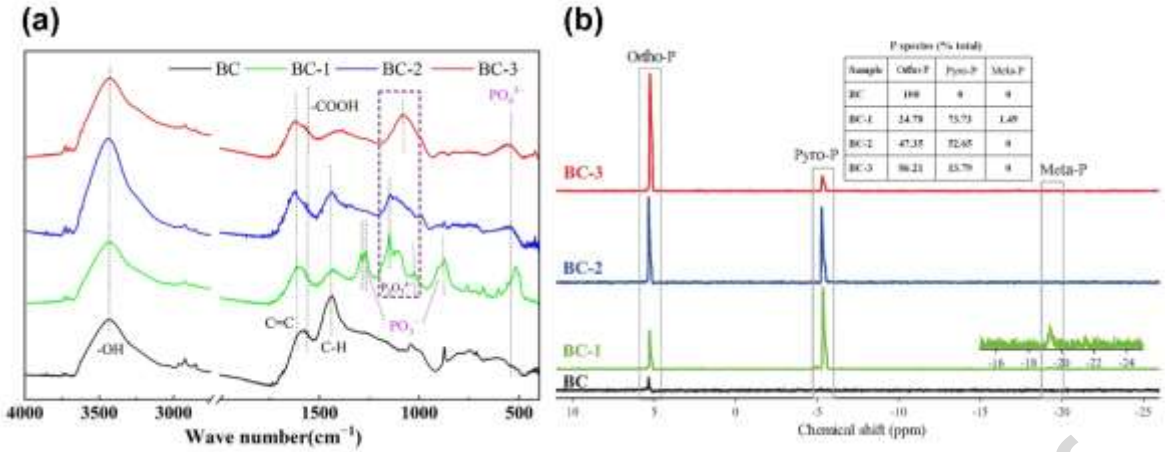

Figure 4. (a) FTIR spectra and (b) solution-state ^{31}P NMR spectra of NaOH-EDTA extracts of biochars prepared from apple tree branches at 500 °C. Spectra are shown for unmodified biochar (BC, black line) and biochars modified with different potassium phosphates: BC-1 (KH_2PO_4), BC-2 (K_2HPO_4) and BC-3 (K_3PO_4). Reprinted (adapted) from Wang et al. [75] with permission from Elsevier, 2022.

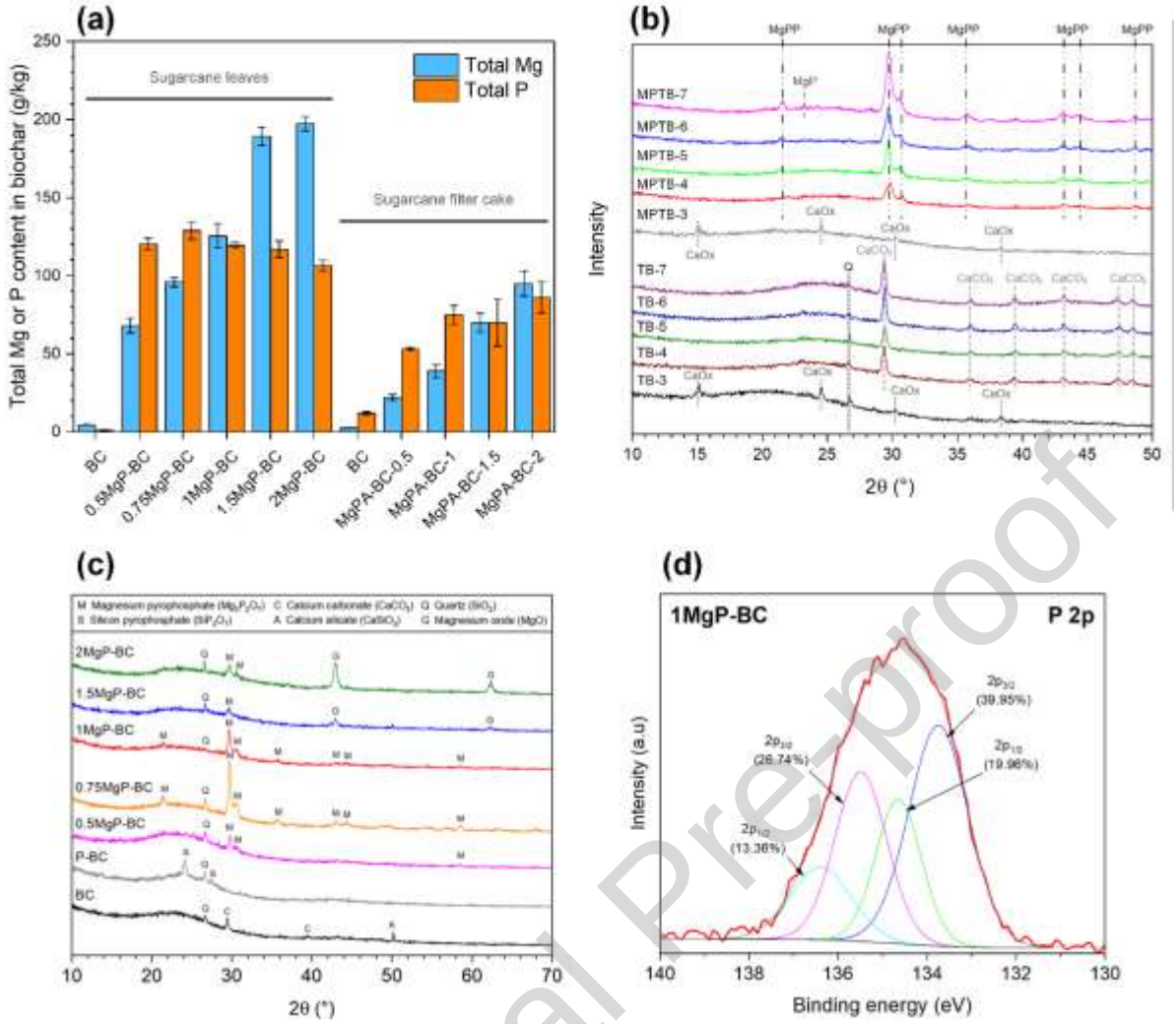

Figure 5. (a) Effect of Mg:P ratio in the pre-treatment process on the total Mg and P contents in biochars prepared from sugarcane leaves and sugarcane filter cake. Figure was prepared using data on sugarcane leaves from Suwanree et al. [11] and sugarcane filter cake from Knijnenburg et al. [80] and Jetsrisuparb et al. [31]; (b) X-ray diffraction patterns of unmodified (TB-3 to TB-7) and Mg/P-modified spent green tea biochars (MPTB-3 to MPTB-7) at 300 to 700 °C. Reprinted (adapted) from Jantapa et al. [81] with permission from Springer Nature, 2024; (c) X-ray diffraction patterns of sugarcane leaf biochars modified with varying Mg:P ratios. Reprinted (adapted) from Suwanree et al. [11] with permission from Springer Nature, 2024; (d) P 2p XPS spectrum of a Mg/P-modified sugarcane leaf biochar (1MgP-BC). Reprinted (adapted) from Suwanree et al. [11] with permission from Springer Nature, 2024.

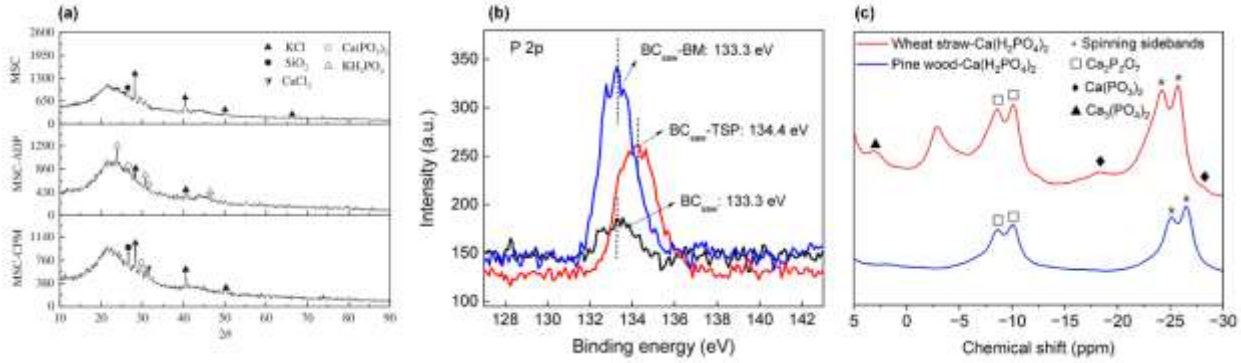

Figure 6. (a) X-ray diffraction patterns of maize straw biochar (MSC) modified with $NH_4H_2PO_4$ (MSC-ADP) and $Ca(H_2PO_4)_2$ (MSC-CPM) produced at 650 C. Reprinted (adapted) from Wang et al. [70] with permission from Springer Nature, 2020; (b) P 2p XPS spectra of sawdust biochar (BC_{saw}) modified with $Ca(H_2PO_4)_2$ (BC_{saw}-TSP) and bone meal (BC_{saw}-BM). Reprinted (adapted) with permission from Zhao et al. [20]. Copyright 2020 American Chemical Society; (c) solid-state ^{31}P NMR spectra of wheat straw and pine wood biochars modified with $Ca(H_2PO_4)_2$ produced at 550 °C. Reprinted (adapted) from Zhang et al. [40] under the Creative Commons Attribution (CC BY) license.

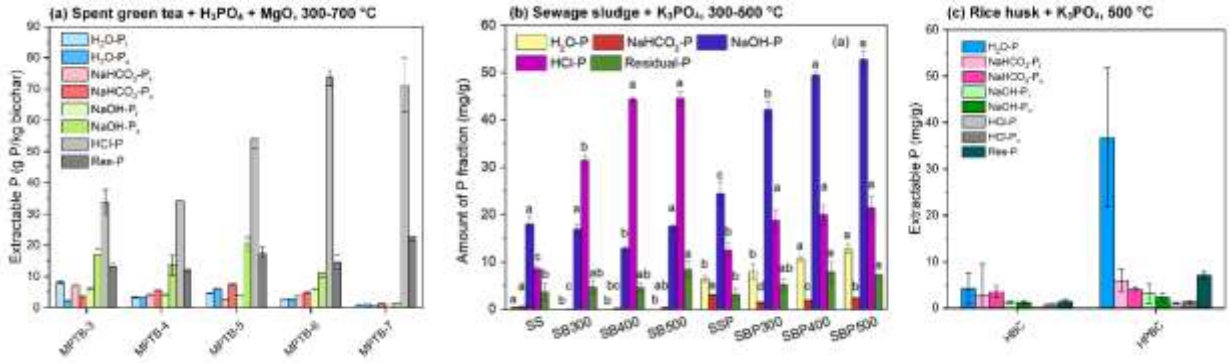

Figure 7. Phosphorus fractionation in modified biochars as determined by sequential (Hedley) extraction: (a) spent green tea biochars co-pyrolyzed with H_3PO_4 and MgO at 300-700 °C (labeled MPTB-3 to MPTB-7). Reprinted (adapted) from Jantapa et al. [81] with permission from Springer Nature, 2024; (b) Sewage sludge (SS), unmodified sewage sludge biochars (SB300 to SB500), and K_3PO_4-modified sewage sludge biochars (SBP300 to SBP500) produced at 300-500 °C. Reprinted (adapted) from Liu and Tian [77] with permission from Elsevier, 2021; (c) Unmodified rice husk biochar (HBC) and K_3PO_4-modified rice husk biochar (HPBC) produced at 500 °C. Figure produced with data from Wu et al. [12].

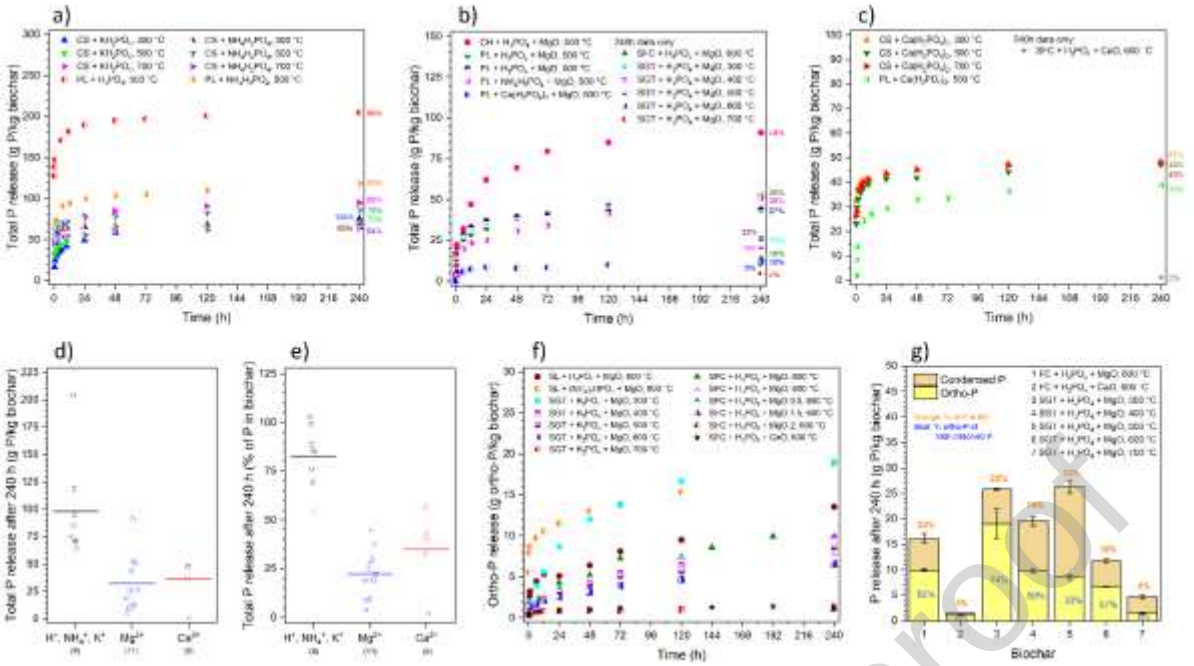

Figure 8. Total P release over 240 hours from biochars modified with (a) H_3PO_4, ammonium and potassium phosphates, (b) magnesium phosphates, (c) calcium phosphates; (d) total P release (g/kg) and (e) relative total P release (%) after 240 h; (f) orthophosphate (PO_4-P) release from modified biochars; (g) orthophosphate and condensed phosphate released after 240 h. Abbreviations and data sources for each feedstock are: Corn stalk (CS) [69]; poultry litter (PL) [60, 63, 93]; coffee husk (CH) [60, 93]; sugarcane filter cake (SFC) [31, 80]; sugarcane leaves (SL) [64]; and spent green tea leaves (SGT) [81].

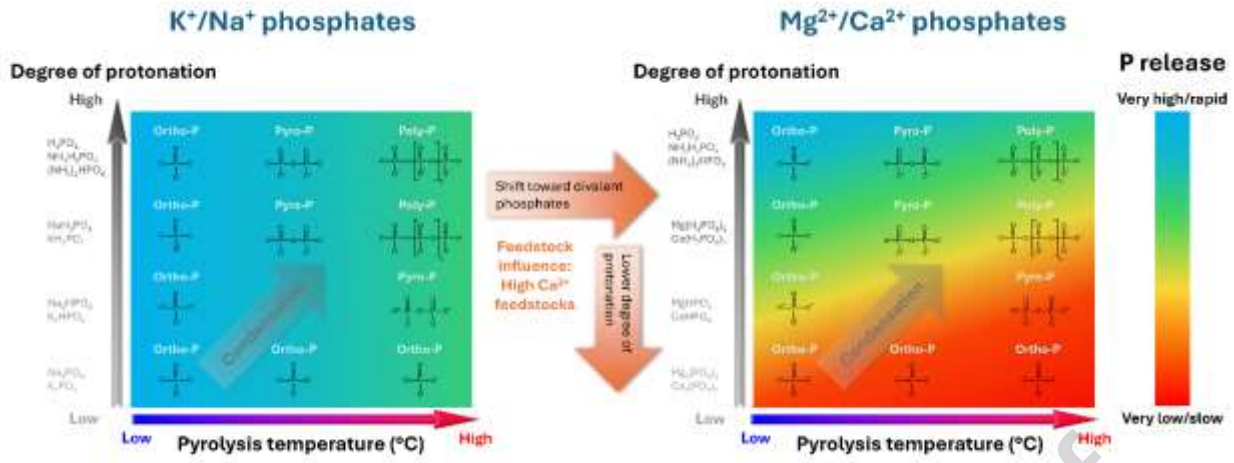

Figure 9. Schematic overview of P transformations and release from phosphate-modified biochars as a function of pyrolysis temperature and the degree of protonation of the phosphate salt additive. The left panel depicts monovalent (K^+/Na^+) phosphates, while the right panel depicts divalent (Mg^{2+}/Ca^{2+}) phosphates; conditions corresponding to H_3PO_4 and ammonium phosphates are included in both maps for comparison. Approximate P species (ortho-, pyro-, and polyphosphate) are indicated in their respective map locations. Color mapping represents the P release kinetics, ranging from very high/rapid (blue) to very low/slow (red). Orange arrows illustrate the influence of biomass feedstock (i.e., high Ca^{2+} content) on P speciation and release.

Table 1. Summary of selected studies on the co-pyrolysis of biomass with phosphoric acid (H_3PO_4). Values after the double slash (//) for yield, total P and biochar pH represent the corresponding values for the unmodified biochar.

Biomass	Additive	Modification conditions	P:biomass ratio (g P/g biomass)	Pyrolysis conditions	Yield (wt%)	Total P (mg P/g biomass)	Biochar pH (-)	Application	Reference
Lignocellulosic biomasses									
Wheat straw	H_3PO_4	Immersion in solution (24h), drying (air)	0.272	500 °C, 1h (stepwise heating)	57 // 32	125 // 1	1.5 // 7.8	Carbon stability	[9]
Peanut shells	H_3PO_4	Wet mixing (60 °C, 2h), drying (65 °C, 24 h)	0.269	500 °C, 2h	-	-	-	Adsorption	[65]
Coffee husk	H_3PO_4	Wet mixing, resting (16h), drying (60 °C)	0.158	500 °C, 2h	65 // 33	146 // 3	2.0 // 11.5	Fertilizer, carbon stability	[60]
Sugarcane leaves	H_3PO_4	Soaking in solution (3h), drying (105 °C, 2 h)	0.083	600 °C, 2h	23 // 23	34 // 7	2.2 // 10.0	Fertilizer	[64]

Animal wastes and biosolids									
Poultry litter	H_3PO_4	Wet mixing, resting (16h), drying (60 °C)	0.158	500 °C, 2h	60 // 39	206 // 24	2.0 // 11.1	Fertilizer, carbon stability	[60, 63]
Poultry manure	H_3PO_4	Acid addition	0.011	300 °C, 2h	-	43 // 19	8.6 // 9.4	Fertilizer	[62]

Table 2. Summary of selected studies on the co-pyrolysis of biomass with ammonium phosphates. Values after the double slash (//) for yield, total P and biochar pH represent the corresponding values for the unmodified biochar.

Biomass	Additive	Modification conditions	P:biomass ratio (g P/g biomass)	Pyrolysis conditions	Yield (wt %)	Total P (mg P/g biomass)	Biochar pH (-)	Application	Reference
Lignocellulosic biomasses									
Peanut shells	$NH_4H_2PO_4$	Wet mixing (60 °C, 2h), drying (65 °C, 24 h)	0.316	500 °C, 2h	-	-	-	Adsorption	[65]

Corn stalk	$NH_4H_2PO_4$	Wet mixing (1h), resting (24h), drying (105 °C, 8h)	0.067	300-700 °C, 1h	65-45 // 45-32	83-119 // 5-8	2.4-2.5 // 7.5-10.2	Fertilizer, carbon stability	[69]
Maize straw	$NH_4H_2PO_4$	Dry mixing	0.024	250-650 °C	-	-	-	Bioenergy	[70]
Pine wood	$NH_4H_2PO_4$	Dry mixing (10 min)	0.016	550 °C, 0.67h	27 // 19	-	-	Fundamental research	[40]
Rice straw	$NH_4H_2PO_4$	Dry mixing (1h)	0.016	350-650 °C, 1h	47-35 // 44-32	-	-	Bioenergy	[67]
Wheat straw	$NH_4H_2PO_4$	Dry mixing (10 min)	0.016	550 °C, 0.67h	28 // 26	-	-	Fundamental research	[40]
Sugarcane leaves	$(NH_4)_2HPO_4$	Soaking in solution (3h), drying	0.083	600 °C, 2h	42 // 23	82 // 7	2.0 // 10.0	Fertilizer	[64]

		(105 °C, 2 h)							
Peanut shells	Ammonium polyphosphate	Wet mixing (60 °C, 2h), drying (65 °C, 24 h)	0.316	500 °C, 2h	-	-	-	Adsorption	[65]
Animal wastes and biosolids									
Poultry litter	$NH_4H_2PO_4$	Dry mixing, moistening, resting (16h), drying (60 °C)	0.135	500 °C, 2h	-	139 // 24	2.8 // 11.1	Fertilizer	[63]

Table 3. Summary of selected studies on the co-pyrolysis of biomass with ammonium phosphates. Values after the double slash (//) for yield, total P and biochar pH represent the corresponding values for the unmodified biochar.

Biomass	Additive	Modification conditions	P:biomass ratio (g P/g biomass)	Pyrolysis conditions	Yield (wt%)	Total P (mg P/g biomass)	Biochar pH (-)	Application	Reference
Lignocellulosic biomasses									

Peanut shell	KH_2PO_4	Dry mixing	0.025-0.098	750 °C, 1h	37-48 // 32	-	-	Carbon stability	[73]
Corn stalk	KH_2PO_4	Wet mixing (1h), resting (24h), drying (105 °C, 8h)	0.057	300-700 °C, 1h	62-43 // 45-32	73-107 // 5-8	6.6-7.8 // 7.5-10.2	Fertilizer, carbon stability	[69]
Apple tree branches	KH_2PO_4	Wet mixing (RT, 24h), dried (60 °C)	0.050	500 °C, 2h	50 // 31	43 // 3	9.2 // 9.0	Adsorption	[75]
Corn stalk	K_2HPO_4	Wet mixing (50 °C, 6h)	0.089	550 C, 2h	-	-	-	Soil remediation	[78]
Apple tree branches	K_2HPO_4	Wet mixing (RT, 24h), drying (60 °C)	0.050	500 °C, 2h	40 // 31	42 // 3	9.5 // 9.0	Adsorption	[75]
Rice husk	K_3PO_4	Wet mixing (RT, 24 h), drying (65 °C)	0.349	500 °C, 2h	61 // 55	62 // 16	11.0 // 8.3	Soil remediation	[12]

Cotton stalk	K_3PO_4	Wet mixing (45 min), drying (80 °C)	0.029-0.117	700 W, 0.25 h (MW)[a]	35-52 // 27	15-28 // -	-	Fertilizer	[79]
Apple tree branches	K_3PO_4	Wet mixing (RT, 24h), drying (60 °C)	0.050	500 °C, 2h	40 // 31	82 // 3	10.0 // 9.0	Adsorption	[75]
Bamboo	K_3PO_4	Wet mixing (80 °C, 6 h)	0.037	350-950 °C, 1h	-	-	8.6-7.5 // 7.5-6.9	Adsorption, carbon stability	[74]
Corncob	K_3PO_4	Wet mixing (80 °C, 6 h), drying (105 °C, 36 h)	0.037	350-950 °C, 0.5h (MW)[a]	64-56 // 49-35	-	-	Carbon stability	[76]
Cotton straw	K_3PO_4	Wet mixing (45 min), drying (vacuum, 90 °C)	0.016	700 W, 0.25h (MW)[a]	46 // 21	-	3.1 // 8.0	Fertilizer	[95]
Animal wastes and biosolids									

Sewage sludge	K_3PO_4	Wet mixing (24 h), drying (60 °C)	2.478	300-500 °C, 3h	64-50 // 59-44	75-97 // 54-71	10.7-11.1 // 7.2-7.5	Fertilizer	[77]

[a] MW: Microwave pyrolysis.

Table 4. Summary of selected studies on the co-pyrolysis of biomass with magnesium phosphates. Values after the double slash (//) for yield, total P and biochar pH represent the corresponding values for the unmodified biochar.

Biomass	Additives	Modification conditions	P:biomass ratio (g P/g biomass)	Pyrolysis conditions	Yield (wt%)	Total P (mg P/g biomass)	Biochar pH (-)	Application	Reference
Lignocellulosic biomasses									
Coffee husk	H_3PO_4 + MgO	Wet mixing, resting (16h), drying (60 °C); Mg:P = 1.0	0.158	500 °C, 2h	64 // 33	177 // 3	5.9 // 11.5	Fertilizer, carbon stability	[60]
Cotton stalk	K_3PO_4 + MgO	Wet mixing (45 min),	0.117	700 W, 0.25h (MW)[a]	49-53 // 27	23-27 // -	-	Fertilizer	[79]

		drying (80 °C); Mg:P = 0.25-0.5							
Spent green tea leaves	H_3PO_4 + MgO	Dry mixing with MgO, soaking in H_3PO_4 solution, drying; Mg:P = 1.0	0.083	300-700 °C, 3h	56-36 // 52-29	103-120 // 7-11	-	Fertilizer	[81]
Sugarcane filter cake	H_3PO_4 + MgO	Dry mixing with MgO, soaking in H_3PO_4 solution, drying; Mg:P = 1.0	0.083	600 °C, 3h	60 // 64	74 // 12	7.7	Fertilizer	[31]
Sugarcane filter cake	H_3PO_4 + MgO	Dry mixing with MgO, soaking in H_3PO_4	0.083	600 °C, 3h	60-65 // -	53-86 // -	-	Fertilizer	[80]

		solution, drying; Mg:P = 0.5-2.0							
Sugarcane leaves	H_3PO_4 + MgO	Dry mixing with MgO, soaking in H_3PO_4 solution (3h), drying (60 °C, overnight); Mg:P = 0.5-2.0	0.083	600 °C, 2h	38-45 // 28	107-129 // 1	4.1-10.0 // 10.0	Adsorption	[11]
Sugarcane leaves	H_3PO_4 + MgO	Dry mixing with MgO, soaking in H_3PO_4 solution (3h), drying (105 °C, 2	0.083	600 °C, 2h	21 // 23	81 // 7	7.3 // 10.0	Fertilizer	[64]

		h); Mg:P = 1.0							
Sugarcane leaves	$(NH_4)_2HPO_4$ + MgO	Dry mixing with MgO, soaking in $(NH_4)_2HPO_4$ solution (3h), drying (105 °C, 2 h); Mg:P = 1.0	0.083	600 °C, 2h	33 // 23	77 // 7	3.6 // 10.0	Fertilizer	[64]
Wheat straw	KH_2PO_4 + $MgCl_2$	Wet mixing (24h), drying (80 °C); Mg:P = 1.0	0.310	600 °C, 2h	-	-	-	Adsorption	[82]
Animal wastes and biosolids									
Poultry litter	H_3PO_4 + MgO	Wet mixing, resting (16h),	0.158	500 °C, 2h	61 // 39	162 // 24	6.1 // 11.1	Fertilizer, carbon stability	[60, 63]

		drying (60 °C); Mg:P = 1.0							
Poultry litter	$NH_4H_2PO_4$ + MgO	Dry mixing, moistening, resting (16h), drying (60 °C); Mg:P = 1.0	0.135	500 °C, 2h	-	135 // 24	6.9 // 11.1	Fertilizer	[63]
Poultry litter	$Ca(H_2PO_4)_2$ + MgO	Dry mixing, moistening, resting (16h), drying (60 °C); Mg:P = 1.0	0.132	500 °C, 2h	-	124 // 24	9.1 // 11.1	Fertilizer	[63]

[a] MW: Microwave pyrolysis.

Table 5. Summary of selected studies on the co-pyrolysis of biomass with calcium phosphates. Values after the double slash (//) for yield, total P and biochar pH represent the corresponding values for the unmodified biochar.

Biomass	Additive	Modification conditions	P:biomass ratio (g P/g biomass)	Pyrolysis conditions	Yield (%)	Total P (mg P/g biomass)	Biochar pH (-)	Application	Reference
Lignocellulosic biomasses									
Wheat straw	$Ca(H_2PO_4)_2$	Immersion in slurry (24h), drying (air)	0.106	500 C, 1h (stepwise heating)	47 // 32	68 // 1	3.9 // 7.8	Carbon stability	[9]
Corn stalk	$Ca(H_2PO_4)_2$	Mixing in solution (1h), resting (24h), drying (105 °C, 8h)	0.066	300-700 °C, 1h	63-45 // 45-32	85-119 // 5-8	3.6-4.0 // 7.5-10.2	Fertilizer, carbon stability	[69]
Sawdust	$Ca(H_2PO_4)_2$	Dry mixing	0.066	500 °C, 2h	-	48 // 1	5.1 // 9.6	Fertilizer, carbon stability, soil	[20]

								remediation	
Switchgrass	$Ca(H_2PO_4)_2$	Dry mixing	0.066	500 °C, 2h	-	58 // 2	5.0 // 8.6	Fertilizer, carbon stability, soil remediation	[20]
Rice straw	$Ca(H_2PO_4)_2$	Wet mixing (2h), drying (105 °C, 24h)	0.053	500 °C, 2h	-	-	7.0 // 10.5	Adsorption	[84]
Rice straw	$Ca(H_2PO_4)_2$	Dry mixing	0.053	500 °C, 1h (stepwise heating)	42 // 36	-	4.3 // 8.6	Carbon stability	[114]
Maize straw	$Ca(H_2PO_4)_2$	Dry mixing	0.024	250-650 °C, -	-	-	-	Bioenergy	[70]
Pine wood	$Ca(H_2PO_4)_2$	Dry mixing (10 min)	0.016	550 °C, 0.67h	28 // 19	-	-	Fundamental research	[40]

Wheat straw	$Ca(H_2PO_4)_2$	Dry mixing (10 min)	0.016	550 °C, 0.67h	28 // 26	-	-	Fundamental research	[40]
Sugarcane filter cake	H_3PO_4 + CaO	Dry mixing with CaO, soaking in H_3PO_4 solution, drying; Ca:P = 1.0	0.083	600 °C, 3h	68 // 64	73 // 12	7.0 // 8.1	Fertilizer	[31]
Animal wastes and biosolids									
Poultry litter	$Ca(H_2PO_4)_2$	Dry mixing, moistened, resting (16h), drying (60 °C)	0.132	500 °C, 2h	-	118 // 24	4.6 // 11.1	Fertilizer	[63]

Table 6. Overview of current limitations and future research needs for phosphate-modified biochar fertilizers.

Category	**Current limitations**	**Future research needs**
1. Advanced characterization	Lacking detail on P transformations within biochar matrix, especially amorphous phases containing condensed phosphates	Employ advanced spectroscopic techniques (e.g., XANES, NMR) to track amorphous P speciation
2. Agronomic efficiency	Limited feedstock variety tested Efficacy limited to lab/pot trials Limited knowledge on interactions between condensed phosphates and biochar	Conduct field trials in real-world conditions Assess overall nutrient performance (e.g., N, P, K) Evaluate polyphosphate/biochar composites as slow release systems in plant trials
3. Scale-up and economics	Significant engineering challenges for scale-up synthesis High cost variability	Optimize synthesis for energy efficiency Conduct comparative cost analysis (pure chemicals vs. waste-derived P sources) Perform life cycle assessment (LCA)

Author contributions:

Jesper T.N. Knijnenburg: Conceptualization, Data curation, Formal analysis, Investigation, Methodology, Software, Visualization, Writing – original draft;

Kaewta Jetsrisuparb: Conceptualization, Methodology, Project administration, Supervision, Validation, Writing – review & editing.

Declaration of Competing Interest

The authors declare that they have no known competing financial interests or personal relationships that could have appeared to influence the work reported in this paper.